MICROBIOLOGY

Targeting the phosphatidylglycerol lipid: An amphiphilic dendrimer as a promising antibacterial candidate

Nian Zhang[1]†, Dinesh Dhumal[2]†, Shanny Hsuan Kuo[3], Shi Qian Lew[3], Pankaj D. Patil[4], Raleb Taher[4], Sanika Vaidya[4], Christina Galanakou[2], Abdechakour Elkihel[2], Myung Whan Oh[3], Sook Yin Chong[3], Domenico Marson[5], Jun Zheng[1], Oleg Rouvinski[4], Williams O. Abolarin[4], Sabrina Pricl[5,6], Gee W. Lau[3]*, Leo Tsz On Lee[1,7,8]*, Ling Peng[2]*

The rapid emergence and spread of multidrug-resistant bacterial pathogens require the development of antibacterial agents that are robustly effective while inducing no toxicity or resistance development. In this context, we designed and synthesized amphiphilic dendrimers as antibacterial candidates. We report the promising potent antibacterial activity shown by the amphiphilic dendrimer **AD1b**, composed of a long hydrophobic alkyl chain and a tertiary amine-terminated poly(amidoamine) dendron, against a panel of Gram-negative bacteria, including multidrug-resistant *Escherichia coli* and *Acinetobacter baumannii*. **AD1b** exhibited effective activity against drug-resistant bacterial infections in vivo. Mechanistic studies revealed that **AD1b** targeted the membrane phospholipids phosphatidylglycerol (PG) and cardiolipin (CL), leading to the disruption of the bacterial membrane and proton motive force, metabolic disturbance, leakage of cellular components, and, ultimately, cell death. Together, **AD1b** that specifically interacts with PG/CL in bacterial membranes supports the use of small amphiphilic dendrimers as a promising strategy to target drug-resistant bacterial pathogens and addresses the global antibiotic crisis.

INTRODUCTION

Bacterial infections are a persistent public health issue and the emergence of antibiotic-resistant microorganisms, especially the so-called ESKAPEE pathogens, poses an increasingly serious threat to global health (*1–5*). ESKAPEE pathogens include *Enterococcus faecium*, *Staphylococcus aureus*, *Klebsiella pneumoniae*, *Acinetobacter baumannii*, *Pseudomonas aeruginosa*, *Enterobacter species*, and *Escherichia coli*. A recent study demonstrated that antimicrobial resistance (AMR) was associated with an estimated 4.95 million deaths and directly caused an estimated 1.27 million deaths worldwide in 2019 (*6*). The emergence of antibiotic-resistant bacteria is attributed to both intrinsic and acquired resistance; the latter promoted by the overuse of antibiotics in agriculture, human health care, and veterinary medicine that leads to gene mutations and the transfer of resistance genes (*7–10*). Prioritizing the development of potent antimicrobial agents that circumvent existing antibiotic resistance mechanisms while reducing vulnerability to the emergence of new resistance mechanisms is an urgent requirement (*11–13*).

Current approaches to addressing AMR encompass the combination of antibiotic agents with adjuvants or alternative therapies including bacteriophages, antibodies, antimicrobial peptides, nucleic acids, and nanoparticles (*14–16*). Among these approaches, amphiphilic dendrimers are emerging as a promising paradigm to combat bacterial AMR (*17–19*). These compounds mimic antimicrobial peptides, exhibiting robust antibacterial efficacy while minimizing the likelihood of resistance development (*20*). Furthermore, their unique dendritic architecture, comprising a central core, branch units, and terminal functional groups, confers inherent stability against enzymatic degradation (*21, 22*) by creating steric hindrance that limits access to enzyme active sites (*23, 24*). In addition, the hydrophobic components and hydrophilic dendritic structures that comprise amphiphilic dendrimers allow their precise design and synthesis toward an optimized hydrophobic-hydrophilic balance to generate potent antibacterial activity, while minimizing adverse effects and drug resistance (*20*).

We have previously evaluated amphiphilic dendrimers for their antibacterial activity. Specifically, these dendrimers consist of a long hydrophobic alkyl chain and a small hydrophilic poly(amidoamine) dendron bearing one of the following charged terminals: primary amine, tertiary amine, guanidine, or carboxylate moieties (*19, 25*). Bearing tertiary amine terminals, **AD1b** (Fig. 1A) is of particular interest because it has the unique advantage of offering selective and potent antibacterial activity against multiple Gram-negative bacteria, with low cytotoxicity. **AD1b** showed no antibacterial activity against the Gram-positive bacterium *S. aureus*. Although the dendrimer bearing primary amine terminals exhibited strong antibacterial activity against both Gram-negative and Gram-positive bacteria, it also had higher cytotoxicity compared to **AD1b**. Contextually, dendrimers bearing guanidine and carboxylate terminals did
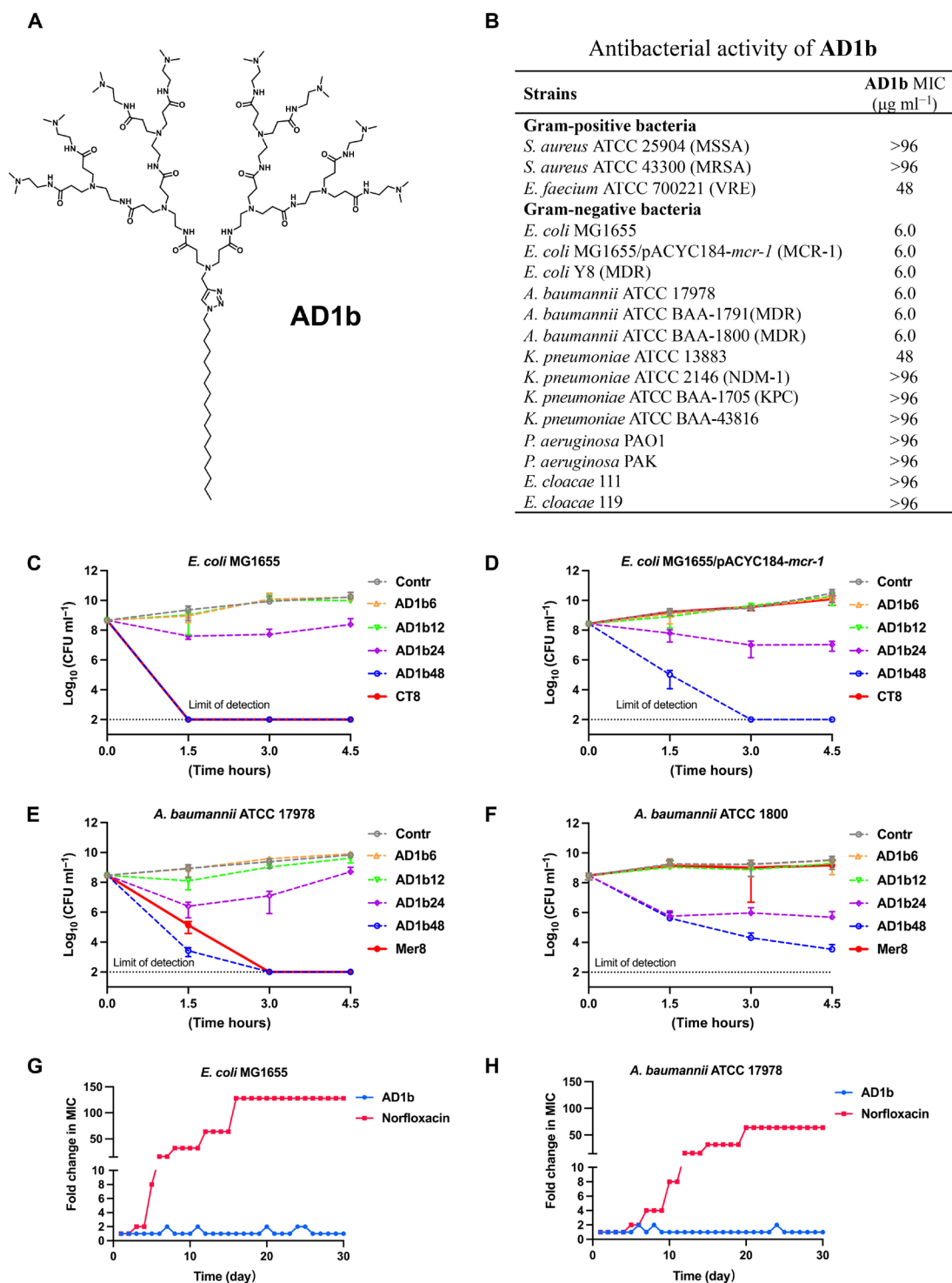
[1]Faculty of Health Sciences, University of Macau, Taipa, Macau, China. [2]Aix-Marseille Universite, CNRS, Centre Interdisciplinaire de Nanoscience de Marseille, UMR 7325, "Equipe Labellisee Ligue Contre le Cancer," 13288 Marseille, France. [3]Department of Pathobiology, University of Illinois at Urbana-Champaign, Urbana, IL, USA. [4]Antimicrobial Discovery Center, Department of Biology, Northeastern University, Boston, MA, USA. [5]Molecular Biology and Nanotechnology Laboratory (MolBNL@UniTS), DEA, University of Trieste, Trieste, Italy. [6]Department of General Biophysics, Faculty of Biology and Environmental Protection, University of Lodz, Lodz, Poland. [7]Cancer Centre, Faculty of Health Sciences, University of Macau, Taipa, Macau, China. [8]Ministry of Education Frontiers Science Center for Precision Oncology, University of Macau, Taipa, Macau, China.
*Corresponding author. Email: ltolee@um.edu.mo (L.T.O.L.); geelau@illinois.edu (G.W.L.); ling.peng@univ-amu.fr (L.P.)
†These authors contributed equally to this work.

A

AD1b

B

Antibacterial activity of **AD1b**

Strains	AD1b MIC ($\mu g\ ml^{-1}$)
Gram-positive bacteria	
S. aureus ATCC 25904 (MSSA)	>96
S. aureus ATCC 43300 (MRSA)	>96
E. faecium ATCC 700221 (VRE)	48
Gram-negative bacteria	
E. coli MG1655	6.0
E. coli MG1655/pACYC184-*mcr-1* (MCR-1)	6.0
E. coli Y8 (MDR)	6.0
A. baumannii ATCC 17978	6.0
A. baumannii ATCC BAA-1791(MDR)	6.0
A. baumannii ATCC BAA-1800 (MDR)	6.0
K. pneumoniae ATCC 13883	48
K. pneumoniae ATCC 2146 (NDM-1)	>96
K. pneumoniae ATCC BAA-1705 (KPC)	>96
K. pneumoniae ATCC BAA-43816	>96
P. aeruginosa PAO1	>96
P. aeruginosa PAK	>96
E. cloacae 111	>96
E. cloacae 119	>96

C *E. coli* MG1655

D *E. coli* MG1655/pACYC184-*mcr-1*

E *A. baumannii* ATCC 17978

F *A. baumannii* ATCC 1800

G *E. coli* MG1655

H *A. baumannii* ATCC 17978

Fig. 1. AD1b is a bactericidal antimicrobial that targets Gram-negative and drug-resistant bacteria effectively. (**A**) Chemical structure of the amphiphilic dendrimer **AD1b**. (**B**) Antibacterial activity of **AD1b** against bacterial strains. MSSA, methicillin-sensitive *S. aureus*; MRSA, methicillin-resistant *S. aureus*; VRE, vancomycin-resistant *Enterococcus*; *mcr-1*, mobilized colistin resistance 1; NDM-1, New Delhi metallo-β-lactamase; KPC, *K. pneumoniae* carbapenemase. Time- and dose-dependent killing assay of **AD1b** on (**C**) *E. coli* MG1655, (**D**) the colistin-resistant *E. coli* (*mcr-1* bearing strain *E. coli* MG1655/pACYC184-*mcr-1*), (**E**) *A. baumannii* ATCC 17978, and (**F**) MDR *A. baumannii* ATCC BAA-1800. Data represent average values ± SD (*n* = 3 per group). Contr, control; **AD1b**6/12/24/48, **AD1b** (6, 12, 24, and 48 $\mu g\ ml^{-1}$, respectively); CT8, colistin (8.0 $\mu g\ ml^{-1}$); Mer8, meropenem at 8.0 $\mu g\ ml^{-1}$. Development of resistance after 30 days of serial passaging using sub-MIC concentrations of **AD1b** and the positive control norfloxacin against (**G**) *E. coli* MG1655 and (**H**) *A. baumannii* ATCC 17978.

not show notable antibacterial activity (*19*). The mechanism underlying the antibacterial efficacy shown by the promising candidate **AD1b** warrants further investigation and validation of its activity in vivo.

In this study, we evaluated the antibacterial activity of **AD1b** against a panel of bacteria including clinically relevant drug-resistant bacteria. **AD1b** exhibited potent antibacterial activity specifically against Gram-negative bacteria, including multidrug-resistant (MDR) *E. coli* and *A. baumannii*. **AD1b** exhibited potent antibacterial activity in vivo against *E. coli* and *A. baumannii* infections in animal models. Our study revealed that **AD1b** exerted its antibacterial effect on bacterial membranes. Specifically, **AD1b** selectively interacts with two crucial membrane phospholipids, namely, phosphatidylglycerol (PG) and cardiolipin (CL). This interaction compromises the integrity of the bacterial membrane, triggering a cascade of detrimental events: disruption of the proton motive force (PMF), metabolic disturbances, and leakage of cellular components, all ultimately culminating in cell death. These findings provide evidence that favors the potential of amphiphilic dendrimers as promising tools in the combat against drug-resistant bacteria responsible for the global antibiotic crisis.

RESULTS

AD1b is selective against Gram-negative bacteria

The antibacterial spectrum is a key characteristic of an antibacterial compound. Broad-spectrum antibacterial compounds can kill a wide range of bacteria, while selective antibacterial compounds are designed to target specific types of bacteria and therefore have a reduced risk of destroying beneficial microorganisms. We therefore first assessed the antibacterial activity of **AD1b** by evaluating its minimum inhibitory concentrations (MICs) against a panel of bacterial strains (Fig. 1B and table S2) using the LB broth microdilution assay. The bacterial strains tested encompassed Gram-positive and Gram-negative bacteria, including ESKAPEE pathogens that represent an increasingly serious threat to global health (*4*, *5*). One example of these pathogens is *A. baumannii* for which approximately 45% of isolates are considered MDR, causing numerous difficult-to-treat infections such as bacteremia, pneumonia, and meningitis (*4*, *26*). Another example is drug-resistant *E. coli,* which cause bloodstream and urinary tract infections that represent a serious public health issue (*27*).

AD1b potently inhibited the growth of various Gram-negative bacteria, including the colistin-resistant *E. coli* strain MG1655 that harbors a plasmid expressing the *mcr-1* gene, uropathogenic MDR *E. coli* Y8, and various MDR *A. baumannii*, with MIC values of 6.0 μg ml^{-1} (Fig. 1B and table S2). However, **AD1b** exhibited weak or no inhibition of Gram-positive bacteria, as shown by the weak inhibition of vancomycin-resistant *E. faecium* (48 μg ml^{-1}) and no inhibition of *K. pneumoniae*, *P. aeruginosa*, *Enterobacter cloacae*, or *S. aureus* (whether methicillin-sensitive or -resistant) even at a high concentration (96 μg ml^{-1}) (Fig. 1B and table S2). Together, these results confirm the selective antibacterial activity of dendrimer **AD1b**.

To further characterize the antimicrobial properties of **AD1b**, we performed dose- and time-dependent killing assays on different strains of *E. coli* and *A. baumannii*. Compared to the clinical antibiotics colistin and meropenem, which showed effective antibacterial activity against sensitive bacterial strains only (*E. coli* MG1655 and *A. baumannii* ATCC 17978) but not the resistant ones (*E. coli* MG1655/

pACYC184-*mcr-1* and MDR *A. baumannii* ATCC BAA-1800), **AD1b** killed all tested Gram-negative bacterial strains, whether antibiotic-sensitive or -resistant, in a concentration- and time-dependent manner (Fig. 1, C to F). Collectively, these results support the potent and superior antibacterial activity of **AD1b** over clinical antibiotics in killing both drug-sensitive and -resistant *E. coli* and *A. baumannii*.

Ideal antibacterial candidates not only demonstrate potent antibacterial activity but also avoid inducing new drug resistance (*28*). Therefore, we evaluated the potential of **AD1b** in developing drug resistance using serial passaging of *E. coli* MG1655 and *A. baumannii* ATCC 17978 at varying concentrations of **AD1b** (0.25 to 4.0 × MIC) for 30 days. As depicted in Fig. 1 (G and H), **AD1b** remained effective against *E. coli* MG1655 and *A. baumannii* ATCC 17978 throughout the 30-day passaging period, while a high level of resistance against the positive control, norfloxacin, was observed for *E. coli* MG1655 and *A. baumannii* ATCC 17978, as shown by the 128- and 64-fold increased MIC values, respectively. These data support the uniquely superior advantage of **AD1b** over other antibiotics with regard to resistance development.

Antibacterial mechanism involves membrane disruption and oxidative stress

The mechanism underlying the potent antibacterial activity of **AD1b** was first examined using scanning electron microscopy (SEM). SEM images revealed notable damage to the cell membrane of *E. coli* caused by and likely responsible for the potent antibacterial activity of **AD1b** (Fig. 2A). Concordantly, **AD1b** caused a significant increase in propidium iodide (PI) staining, indicating a compromised *E. coli* membrane comparable to that caused by the membrane-disrupting antibiotic colistin (Fig. 2B and fig. S1). These data suggest that **AD1b** can act as a membrane disruptor, altering the integrity and morphology of the bacterial membrane.

The disruption of the bacterial membrane can be reflected by the perturbation of the PMF (*29*–*31*). We hence examined the membrane dysfunction caused by **AD1b** by measuring the membrane potential ($\Delta\Psi$) and the transmembrane proton gradient (ΔpH). We first assessed $\Delta\Psi$ changes in bacteria upon treatment with **AD1b** using the membrane potential–sensitive dye, 3,3′-dipropylthiadicarbocyanine iodide [DiSC$_3$(5)] and valinomycin, which dissipates $\Delta\Psi$ by equilibrating the potassium gradient, as the positive control (*32*). Treatment with **AD1b** and valinomycin significantly increased DiSC$_3$(5) fluorescence in *E. coli* cells (Fig. 2C and fig. S2A). We then investigated the impact of **AD1b** on ΔpH changes using the fluorescent pH-sensitive dye 2′,7′-bis-(2-carboxyethyl)-5-(and-6)-carboxyfluorescein acetoxymethyl ester (BCECF-AM). The results depicted in Fig. 2D and fig. S2B demonstrate that changes in bacterial ΔpH occurred in a dose- and time-dependent manner upon **AD1b** treatment. Together, these findings indicate a significant dissipation of bacterial PMF caused by **AD1b**, providing further support for its membrane disruption properties.

Taking into account the observed alteration of membrane integrity caused by **AD1b**, we hypothesized that it also affected the respiratory chain and energy metabolic pathways within the cytoplasmic membrane. We thereby examined the activity of the electron transport chain (ETC) using the tetrazolium salt iodonitrotetrazolium chloride (INT) that reduces to red insoluble formazan by respiratory chain dehydrogenase (*33*). The membrane-disruptive antibiotic colistin was used as a positive control. Similar to colistin, **AD1b** caused
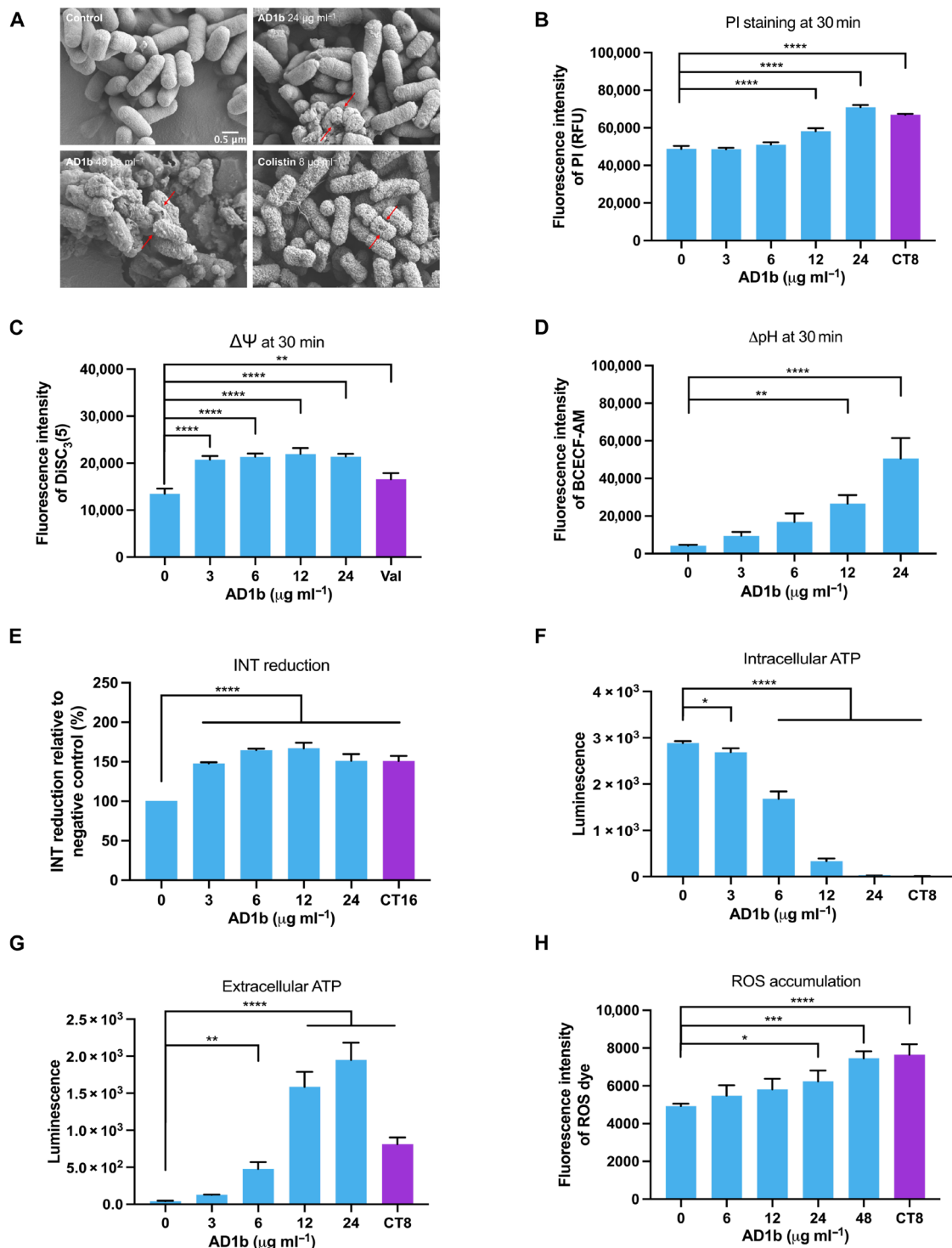
Fig. 2. AD1b disrupts bacterial membrane and leads cell lysis. (**A**) SEM of *E. coli* MG1655 treated with **AD1b** for 30 min. The red arrows represent membrane-damaged cells. Each treatment was viewed using a ×20,000 magnification. (**B**) Inner membrane permeability of *E. coli* MG1655 treated with **AD1b** for 30 min. Colistin (8.0 μg ml^{-1}) was the positive control. Data are average values ± SD (*n* = 3 per group) and analyzed using a one-way analysis of variance (ANOVA). (**C**) Dissipated membrane potential ΔΨ in *E. coli* MG1655 treated with **AD1b** for 30 min. Valinomycin (5.0 μM) was used as a positive control. (**D**) Dissipated ΔpH in *E. coli* MG1655 treated with increasing concentrations of **AD1b** for 30 min. (**E**) Increased cell respiration in *E. coli* MG1655 treated with **AD1b** for 1.0 hour, detected by INT reduction assay. (**F**) Increasingly reduced intracellular ATP levels in *E. coli* MG1655 treated with increasing concentrations of **AD1b** for 1.5 hours. (**G**) Increasing extracellular ATP levels in *E. coli* MG1655 treated with increasing concentrations of **AD1b** for 1.5 hours. (**H**) Increasing ROS accumulation in *E. coli* MG1655 treated with increasing concentrations of **AD1b** for 1.5 hours. Data are average values ± SD (*n* = 3 per group) and analyzed using a one-way ANOVA, *$P < 0.05$, **$P < 0.01$, ***$P < 0.001$, and ****$P < 0.0001$.

a significant increase in INT reduction in *E. coli* (Fig. 2E). These results are consistent with previous studies suggesting that bactericidal agents are associated with accelerated respiration (*34*).

The loss of important cellular constituents, such as adenosine 5′-triphosphate (ATP) and proteins, is a common mechanism shared by many membrane-disruptive agents (*29*). Using the BacTiter-Glo assay, we found that **AD1b** caused a significant decrease in intracellular ATP levels, similar to that induced by the membrane-disruptive drug colistin (Fig. 2F). Furthermore, **AD1b** caused a marked increase in extracellular ATP levels in *E. coli* cells after 1.5 hours (Fig. 2G), as well as extracellular proteins, as shown by bicinchoninic acid assay (fig. S3).

Loss of ATP can cause an imbalance in the cellular redox state, resulting in the accumulation of reactive oxygen species (ROS) and oxidative stress. This represents a common killing mechanism for bactericidal antibiotics (*35*). Accordingly, we assessed ROS accumulation in *E. coli* treated with **AD1b** using the ROS indicator 6-carboxy-2′,7′-dichlorodihydrofluorescein diacetate (carboxy-H$_2$DCFDA). Similar to colistin, **AD1b** induced significant ROS accumulation in *E. coli* cells, which correlated with their killing effect (Fig. 2H). In addition, we examined the MIC of **AD1b** in an anaerobic environment and in the presence/absence of glutathione, respectively. However, we did not observe any changes in the MIC values (table S3). Therefore, the bactericidal activity of **AD1b** could mainly be attributed to membrane disruption and subsequent events caused by membrane dysfunction. These results collectively demonstrate **AD1b**-induced loss of important cellular components and oxidative stress in bacterial cells that ultimately leads to their death.

AD1b targets the phospholipids PG and CL

To further investigate the interaction of **AD1b** with the bacterial membrane, we assessed **AD1b** activity following cotreatment with the three main components of the bacterial membranes: phosphatidylethanolamine (PE), PG, and CL. As a control, we used phosphatidylcholine (PC), which is expressed at low levels in bacteria but is abundant in mammalian cell membranes. Results obtained from the checkerboard assay showed that the anionic phospholipids PG and CL markedly inhibited the antibacterial activity of **AD1b** against *E. coli* in a dose-dependent manner (Fig. 3A and fig. S4). The zwitterionic phospholipids PE and PC, as well as lipopolysaccharide (LPS) and peptidoglycan (PGN), had only negligible effects on the antibacterial activity of **AD1b** (Fig. 3A and fig. S4). These results implicate electrostatic interactions between cationic **AD1b** and anionic membrane phospholipids.

Considering the positive charge of **AD1b**, we wondered whether it could target the LPS of Gram-negative bacteria, in a similar manner to colistin. Supplementation with purified LPS (from *E. coli*) protected the *E. coli* culture from damage by colistin but had no effect on **AD1b** activity. We also tested **AD1b** against the LPS-deficient isogenic mutant strain lpxA of *A. baumannii* and *E. coli* WO153 that expresses less LPS. **AD1b** showed no change in MIC values for these strains (table S4), suggesting an LPS-independent mode of action.

Next, we performed molecular dynamics (MD) simulations at atomistic resolution to evaluate the molecular interaction between **AD1b** and the main bacterial phospholipids. Different fully solvated systems were studied, each containing an **AD1b** monomer and one of the studied (phospholipids PE, PG, CL, or PC). Over short periods of time (<50 ns), simulated anionic phospholipids PG and CL formed very stable complexes with **AD1b**, which were created shortly after the initial random collision between the two molecules. Similar forces underlie these interactions, as shown in Fig. 3B for PG, with the formation of the complex strongly depending on salt bridges between the negatively charged phosphate moiety of the lipid and the positively charged tertiary amines of **AD1b**. Following complex formation, this strong association is further stabilized by minimizing the solvent-exposed surface of the lipid tails and the aliphatic portion of **AD1b**. Notably, simulations performed with the zwitterionic phospholipids PE and PC produced no stable complex, even upon extending the MD simulations to microseconds. Transient complexes did emerge upon random collision of the two molecules, which were driven by the interaction of their aliphatic tails but had a very short lifespan of just a few nanoseconds (10 ± 4 ns). These systems were unstable because of the absence of strong electrostatic driving forces.

Simulations of stable complexes between anionic lipids and **AD1b** were further characterized to determine their binding enthalpy using the molecular mechanics/Poisson-Boltzmann surface area (MM/PBSA) approach (*36*). The results showed that **AD1b** binds PG with a favorable enthalpy change of −3.31 ± 0.25 kcal mol^{-1}, while its complex with CL presents an enthalpy change of −4.95 ± 0.32 kcal mol^{-1}. The more negative and therefore more favorable change in binding enthalpy found in the CL complex can be easily explained by the presence of two negatively charged phosphate groups in CL, which allow for a stronger interaction with positively charged **AD1b**.

We then used isothermal titration calorimetry (ITC) to study the molecular interaction between **AD1b** and PG/PC/PE, choosing to omit CL that is synthesized from two PG molecules and is expressed at low levels in bacteria (*37*). A direct titration indicated that PG bound to **AD1b** with a favorable enthalpy change of −44.9 ± 0.4 kcal mol^{-1} at 25°C (fig. S5A and table S5). This experiment also indicated tight binding between PG and **AD1b**, with a binding affinity too high to be determined by direct titration (fig. S5A). A competitive (displacement) ITC assay according to a reported procedure (*38*) that measures high-affinity molecular interactions using a weak competitor that binds to the same site on the macromolecule helped overcome this issue. We selected BMS-833923 (BMS) as the weak competitor of **AD1b** due to its specific binding to PG with moderate binding affinity (*39*). Thermodynamic parameters calculated after direct titration of BMS into PG were $\Delta H = −7.94$ kcal mol^{-1}, $K_B = 2.44 \times 10^5$ M, and $n = 1.04$ (fig. S5B and table S5). We performed a competitive ITC assay by titration of **AD1b** in PG + BMS at 25°C. The results yielded a strong binding affinity between **AD1b** and PG with a K_D of 3.51 ± 0.79 × 10^{-9} M, a binding enthalpy of −49.2 ± 1.1 kcal mol^{-1}, and a stoichiometric ratio of ~0.049 for **AD1b**/PG (Fig. 3C, fig. S5C, and table S5). In contrast, no significant binding was observed between **AD1b** and PC, PE, or Hepes buffer (fig. S5, D to F). These findings are consistent with the checkerboard assay, supporting **AD1b** targeting PG in bacterial membranes.

We also used computer modeling to study the interaction between **AD1b** and Gram-negative bacterial membranes. For this, we followed our recently established protocol based on MD simulations (*19*). The modeling was initiated by randomly placing **AD1b** monomers in a water environment above the representative symmetric membrane composed of PE, PG, and CL in a 70:20:5 ratio. As the MD simulation progressed, the **AD1b** amphiphiles moved toward the surface of the bacterial membrane, where they could aggregate into small clusters (Fig. 3D, top). These clusters shielded the
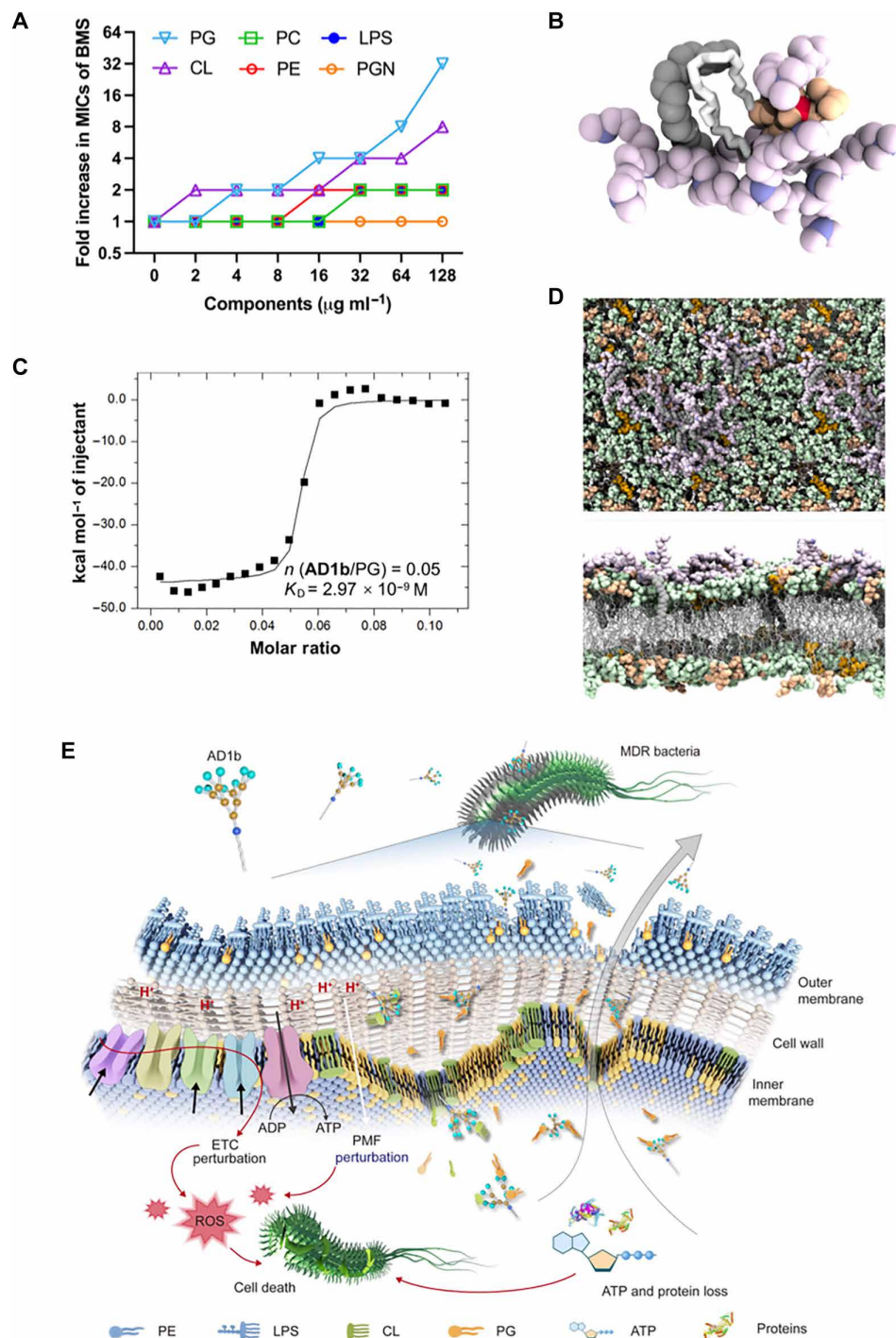
Fig. 3. AD1b targets the bacterial membrane phospholipids PG and CL. (**A**) Checkerboard assay results showed that exogenous addition of PG and CL significantly increased the MIC values of **AD1b** against *E. coli* MG1655. (**B**) The molecular complex of PG and **AD1b**. The C_{18} hydrocarbon chains and dendritic portions are represented in gray and light plum spheres, whereas the positively charged nitrogen atoms are highlighted in a darker plum. The polar headgroup of PG is represented as light orange spheres, with the phosphorous atom highlighted in red. The hydrophobic tails are represented as light gray tubes. (**C**) Competitive ITC analysis of the interaction between **AD1b** and PG. **AD1b** (50 μM) was titrated into 100 μM PG + 10 μM BMS-833923 (BMS). Equilibrium dissociation constant, $K_D = 2.97 \times 10^{-9}$ M; number of binding sites, $n = 0.050$; molar binding enthalpy, $\Delta H = -48.1$ kcal mol^{-1}; $P < 0.0001$. (**D**) Computer modeling of the interaction between **AD1b** and Gram-negative bacterial membrane: initial formation of nanoclusters on the surface of the membrane (top) and final stage with all the hydrophobic tails inserted into the bacterial membrane (bottom). The color label of **AD1b** is the same as above. The lipid hydrophobic tails are represented as light gray tubes, while the polar heads are represented as light green, light orange, and dark orange spheres for PE, PG and CL, respectively. (**E**) **AD1b** bactericidal mode of action. The **AD1b** molecules initially amass on the membrane due to favorable electrostatic and polar interactions. The cationic **AD1b** binds to the anionic phospholipids PG and CL, resulting in membrane disruption, which impairs the normal functioning of the ETC and PMF and leads to the accumulation of ROS, causing the release of cellular components. ADP, adenosine 5′-diphosphate.

hydrophobic tails of the molecules from water and facilitated a strong binding between the positively charged dendrons and the negatively charged bacterial membrane via cooperative and multivalent electrostatic interactions. However, as the simulation time increased further, the **AD1b** clusters were found to disassemble and spread throughout the upper leaflet of the membrane. This crawling process ultimately ended with the complete insertion of the hydrophobic tails of the **AD1b** molecules into the lipid bilayer (Fig. 3D, bottom), ultimately resulting in robust antibacterial activity. Collectively, these findings provide further evidence of **AD1b** causing bacterial membrane disruption by targeting the membrane phospholipids PG and CL, resulting in PMF disruption, metabolic disturbance, and leakage of cellular components that ultimately kill bacteria (Fig. 3E).

AD1b has excellent safety profiles in vitro and in mice

The promising results obtained from cell-based experiments encouraged us to further examine the therapeutic potential of **AD1b** in animal models of infectious diseases. Before the animal study, it was important to assess the in vitro cytotoxicity, in vivo safety profile, and pharmacokinetic properties of **AD1b**.

We first assessed the cytotoxicity of **AD1b** on mammalian cells using the PrestoBlue test and the lactate dehydrogenase (LDH) assay. The PrestoBlue assay examines metabolic toxicity by assessing cell viability, whereas the LDH test evaluates toxicity associated with cell membrane integrity by measuring LDH release. **AD1b** showed no detectable metabolic toxicity or membrane damage at concentrations over 30-fold the MIC (i.e., 217 μg ml^{-1}) on all mammalian cells tested, including mouse macrophage cells (RAW264.7), mouse fibroblast cells (NIH 3T3), Chinese hamster ovary cells (CHO K1), and African green monkey kidney cells (Vero) (Fig. 4, A and B).

AD1b was further evaluated with respect to lysis of red blood cells. The hemolysis assay using sheep red blood cells revealed a very low hemolytic activity (~10%) of **AD1b**, even at 256 μg ml^{-1} (over 40-fold the MIC), similar to the membrane-disrupting antibiotic colistin (fig. S6). Together, these data highlight the good potential of **AD1b** as an efficient yet safe antibacterial candidate.

For acute in vivo toxicity assessment, CD-1 mice were inoculated intraperitoneally twice daily with **AD1b** (5.0 mg kg^{-1}) for 7 days, with control mice challenged with sterile phosphate-buffered saline (PBS). Mouse weight did not show significant differences between treatment groups during the exposure period (fig. S7). We found no histopathological evidence of treatment-associated toxicity in the liver, kidneys, spleen, heart, or lungs (Fig. 4C).

We further examined biostability and biodistribution of the intraperitoneally administered Cyanine7.5-conjugated **AD1b** (Cy7.5-**AD1b**) over 72 hours using an IVIS SpectrumCT imaging system, in control mice, as well as during acute pneumonia and bacteremia mediated by *E. coli* AR bank 0349 (table S1). Intraperitoneally injected Cy7.5-**AD1b** exhibited favorable biodistribution and continued to circulate well beyond 72 hours after injection when administered alone (Fig. 4D), or in the context of either *E. coli*–mediated bacteremia or pneumonia infection [24 hours after infection (hpi); Fig. 4E], with the fluorescence signals accumulating in all major organs (Fig. 4F and fig. S8). Prolonged stability of **AD1b** indicates its recalcitrance to degradation by host and bacterial proteases. Fluorescence signals, particularly those in the heart, were artificially low because of blood loss during organ harvesting.

Effective in vivo antibacterial activity

Encouraged by excellent safety profile, stability, and biodistribution, we then examined the therapeutic potential of **AD1b** in mouse models of bacteremia, acute pneumonia, and peritonitis-sepsis (Fig. 5A). These infection models are frequently used to simulate human infection and explore the therapeutic effect of drugs. We chose the two pathogenic bacterial strains *E. coli* AR bank 0349 (*40*) and *A. baumannii* W47919 (*41*, *42*), both drug-resistant clinical isolates from human. The bacteremia infection and acute pneumonia infection mouse models were first infected with a high dose of *E. coli* AR bank 0349 or *A. baumannii* W47919 (Fig. 5, A and D). This was followed 2.0 hpi by administration of **AD1b** twice daily for 1 day in the bacteremia infection model and for 2 days in the acute pneumonia infection model, using a saline vehicle and the antibiotic tigecycline as the negative and positive controls, respectively. Notably, **AD1b** treatment substantially reduced the bacterial load in both models compared to vehicle treatment (Fig. 5, B, C, E, and F). In the bacteremia model (Fig. 5D), **AD1b** at the low dose of 5.0 mg kg^{-1} significantly decreased the bacterial burden by 1000-fold, achieved by tigecycline only at the high dose of 50 mg kg^{-1} (Fig. 5, E and F). Similarly, in the acute pneumonia model, the same low dose of **AD1b** (5.0 mg kg^{-1}) achieved approximately a 1000-fold reduction in bacterial load for *E. coli* AR bank 0349 as tigecycline (50 mg kg^{-1}) in the lungs (Fig. 5B) and 100-fold in *A. baumannii* W47919 (Fig. 5C). In the peritonitis-sepsis model (Fig. 5G), **AD1b** treatment (5.0 mg kg^{-1}) produced notably higher survival rates in the *E. coli* AR bank 0349– and *A. baumannii* W47919–infected mice compared to vehicle treatment (Fig. 5, H and I). Collectively, these results confirm the potency of **AD1b** as an antibacterial agent in vivo.

DISCUSSION

The ever-growing antibiotic resistance is alarming and requires the rapid development of antibacterial agents with robust efficacy yet zero toxicity or risk of resistance development (*1*, *2*). Amphiphilic dendrimers are emerging as a promising solution to combat antibiotic resistance (*20*). They comprise distinct hydrophobic and hydrophilic moieties within their dendritic structures that can be designed and synthesized precisely to ensure potent activity and avoid inducing cellular toxicity and new resistance. In this context, we have developed **AD1b**, composed of a hydrophobic C$_{18}$ alkyl chain and a hydrophilic poly(amidoamine) dendron carrying tertiary amine terminals (*19*). **AD1b** was found to be particularly attractive as it selectively and effectively killed certain Gram-negative bacteria, even drug-resistant strains, at a very low dose (MIC = 6.0 μg ml^{-1}), yet with reasonable safety and negligible cytotoxicity below 217 μg ml^{-1} (over 30-fold the MIC). Our mechanistic studies showed that **AD1b** caused bacterial membrane disruption by targeting membrane phospholipid PG, resulting in the disruption of the PMF, metabolic disturbance, and leakage of cellular components that ultimately killed bacteria.

Because bacterial membranes have a distinct composition compared to mammalian membranes, selective membrane-targeted drugs are a promising approach to developing antibacterial agents (*29*, *43*). Anionic phospholipids and, in particular, PG are abundant in *E. coli* cell membranes where they constitute ~20 to 25% of total lipids (*44*), compared to only ~1% in mammalian cell membranes (*45*). Therefore, compounds selectively targeting PG are appealing
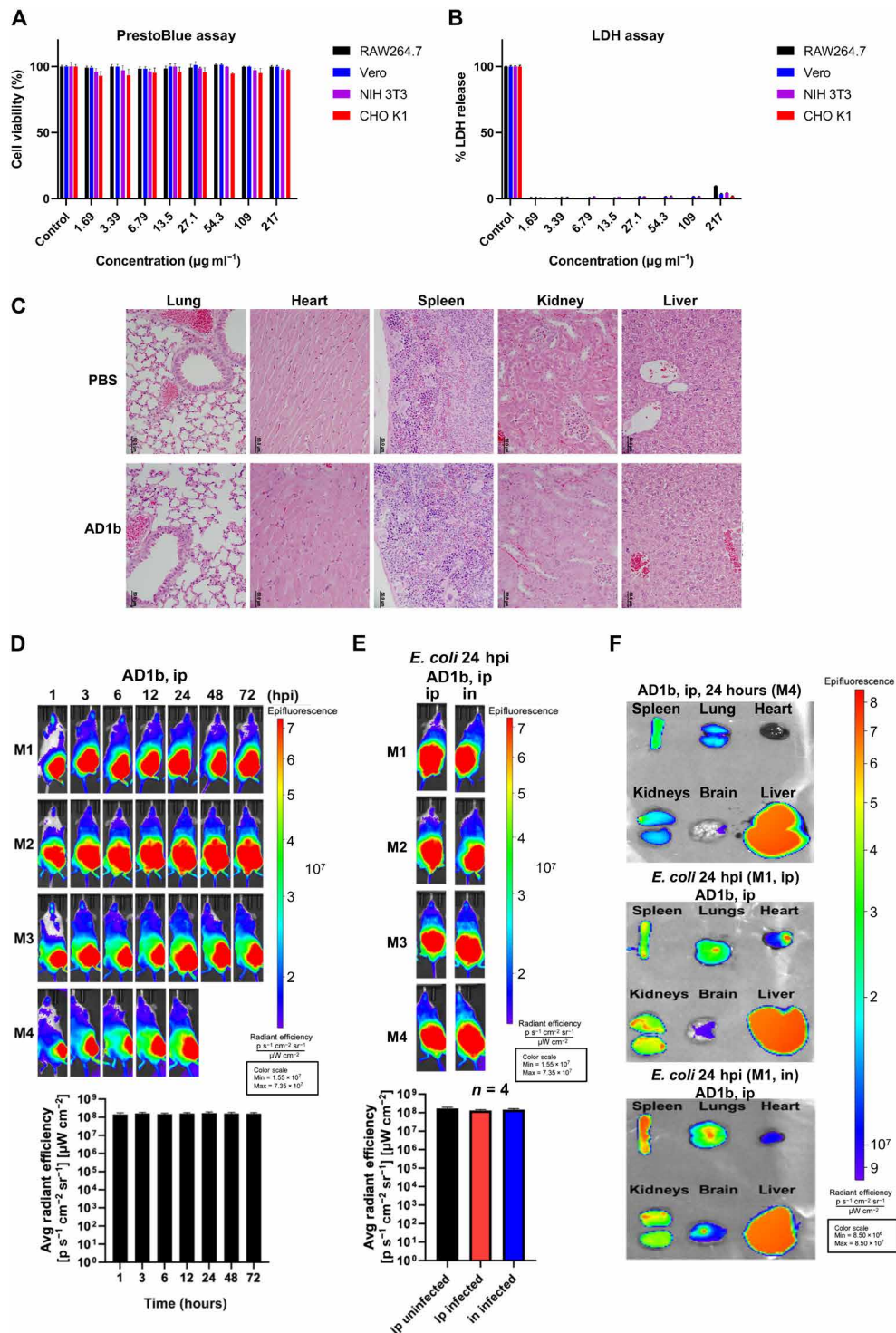
Fig. 4. Safety evaluation and pharmacokinetic properties of AD1b. (**A**) Cytotoxicity evaluation of **AD1b** on mouse macrophage cells (RAW264.7), African green monkey kidney cells (Vero), mouse fibroblast cells (NIH 3T3) cells, and Chinese hamster ovary cells (CHO K1) at 48 hours after treatment using the PrestoBlue assay. (**B**) Evaluation of membrane damage by **AD1b** on RAW264.7, Vero, NIH 3T3, and CHO K1 cells using LDH assay. Lysis buffer provided in the commercial LDH assay kit was used as positive control (control). (**C**) Representative hematoxylin and eosin–stained histopathological images of major organs from CD-1 mice after 7 days of intraperitoneal injections of **AD1b** (5.0 mg kg^{-1}, twice daily). Magnification, ×400. (**D**) Biostability and biodistribution of intraperitoneally injected Cy7.5-**AD1b** (50 μg of Cy7.5) over 72 hours in CD-1 mice (n = 3 to 4) imaged by an IVIS SpectrumCT imager. (**E**) Biostability and biodistribution of intraperitoneally injected Cy7.5-**AD1b** (50 μg of Cy7.5) over 24 hours in CD-1 mice (n = 3 to 4) with *E. coli* bacteremia [intraperitoneally (ip); 5.2 × 10^7 colony-forming units (CFU)] or acute pneumonia [intranasally (in); 1.1 × 10^8 CFU] imaged by an IVIS SpectrumCT imager. (**F**) Major organs were excised from representative mice at 24 hpi, imaged in a rainbow color scale, and quantified. M1 is mouse #1 from (E). M4 is mouse #4 from (D).
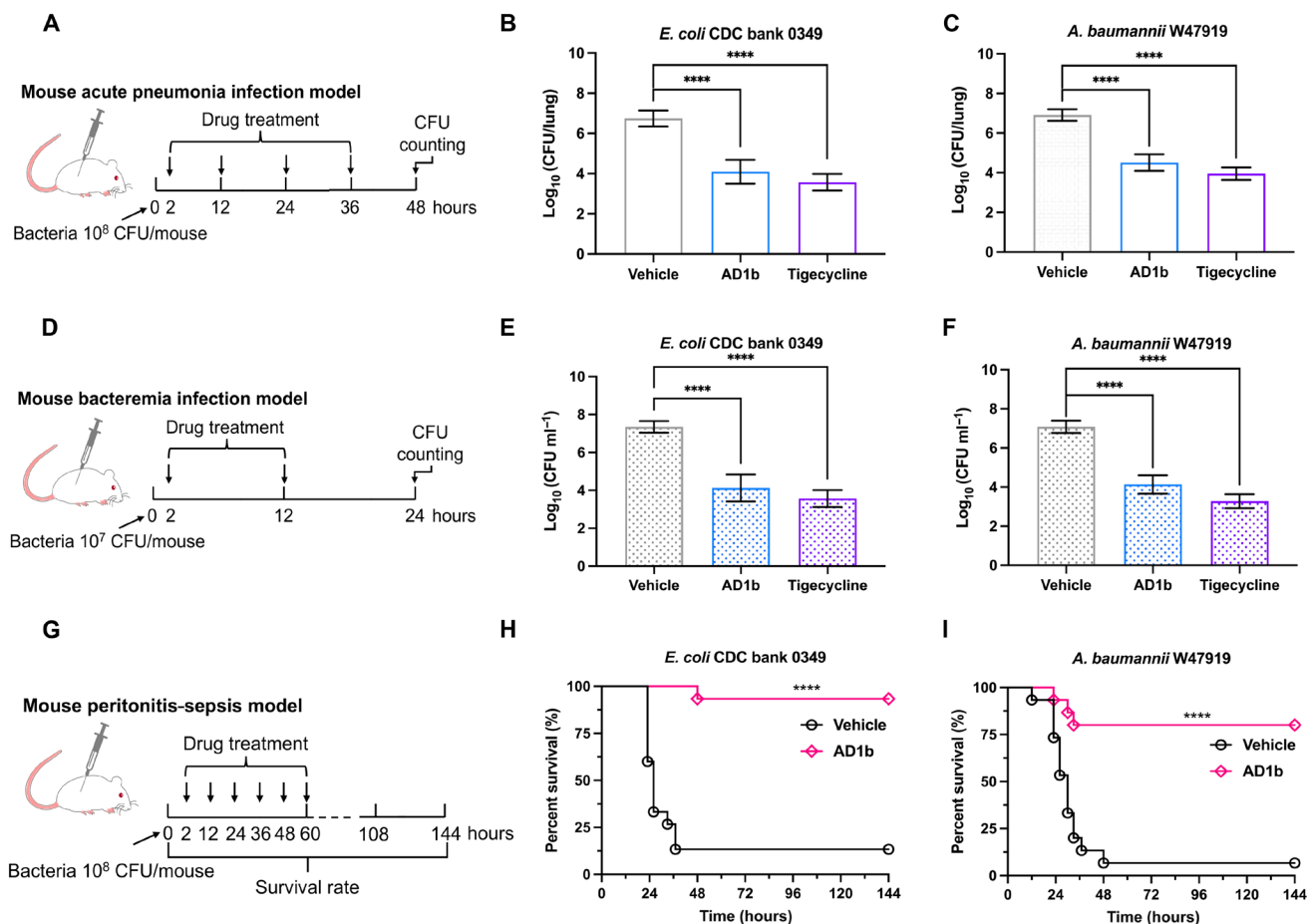
Fig. 5. In vivo antibacterial activity of AD1b. (A to C) Mouse acute pneumonia infection ($n = 8$ in each group). Mice were intranasally infected with drug-resistant *E. coli* AR bank 0349 (3.8×10^8 CFU per mouse) and *A. baumannii* W47919 (2.0×10^8 CFU per mouse). Infected animals were treated twice daily (first treatment at 2 hpi) with PBS (intraperitoneally), **AD1b** (5 mg kg^{-1}) (intraperitoneally), and tigecycline (50 mg kg^{-1}) [subcutaneously (SQ)] before euthanasia at 48 hours. **(D to F)** Mouse bacteremia infection model ($n = 6$ in each group). Mice were intraperitoneally infected with *E. coli* AR bank 0349 (7.8×10^7 CFU per mouse) and *A. baumannii* W47919 (5.3×10^7 CFU per mouse). Infected animals were treated twice daily with PBS (intraperitoneally), **AD1b** (5 mg kg^{-1}) (intraperitoneally), and tigecycline (50 mg kg^{-1}) (subcutaneously) before euthanasia at 24 hours. **(G to I)** Mouse peritonitis-sepsis mortality studies ($n = 15$ in each group). Survival rates of mice intraperitoneally infected with *E. coli* AR bank 0349 (4.3×10^8 CFU per mouse) and *A. baumannii* W47919 (2.5×10^8 CFU per mouse). Infected animals were treated twice daily with PBS (intraperitoneally) or **AD1b** (5.0 mg kg^{-1}) (intraperitoneally) for 3 days and monitored 144 hours. Data in (B), (C), (E), and (F) are average values ± SD. All data were analyzed using an unpaired, two-tailed Student's *t* test. ****$P < 0.0001$. Mouse survival was analyzed with the Kaplan-Meier log rank survival test in the GraphPad Prism version 9.0.2 software.

antibacterial candidates that can kill bacteria while showing low toxicity in mammalian cells. For example, the antibiotic daptomycin targets PG and therefore exhibits potent antibacterial activity against various Gram-positive bacteria with low cytotoxicity toward mammalian cells (*46*, *47*). This example highlights the promising therapeutic perspective for antibacterial agents targeting PGs.

We compared **AD1b** with daptomycin and other candidates targeting PG (Table 1) and found that **AD1b**, similarly to these PG-targeting drug candidates (*30*, *31*, *48*), interacted with anionic phospholipids through electrostatic interactions. Computational experiments provided support for the mechanistic concept of **AD1b** molecules initially binding to the bacterial membrane and accumulating there through favorable electrostatic and polar interactions. Subsequent self-assembly into nanoclusters, due to their amphiphilic nature, allows the rearrangement and redistribution of dendrimer molecules around the bacterial surface. This arrangement enables the long hydrophobic tails of **AD1b** to fully integrate into the lipid

bilayer through collective hydrophobic interactions that ultimately initiate antibacterial activity via membrane disruption.

Further thermodynamic data indicate that each **AD1b** binds to 20 PG molecules with the highest binding affinity ($K_D = 3.51 \pm 0.79 \times 10^{-9}$ M) among the PG-targeting drugs (Table 1). **AD1b** had negligible and much lower cytotoxicity [half-maximal inhibitory concentration (IC$_{50}$) > 100 μM] compared to other PG-targeting compounds. This low cytotoxicity indicates that developing amphiphilic dendrimers as antibacterial agents with high PG binding affinity is an appealing strategy. In particular, targeting PG provides a promising perspective in the design of next-generation antibacterial agents to address the worldwide crisis of antibiotic resistance.

AD1b presented here has a rather selective antibacterial activity spectrum, showing much more effective activity against Gram-negative bacteria than Gram-positive bacteria (Fig. 1B and table S2). Regarding the insensitivity of certain Gram-negative bacteria to **AD1b**, the diversity of membrane phospholipids among different

Table 1. Summary of PG-targeted drugs. AMG, α-mangostin; IBC, isobavachalcone; G$^+$, Gram-positive bacteria; G$^-$, Gram-negative bacteria.

Drugs	Daptomycin	SLAP-S25	AMG and IBC	BMS	AD1b
Category	Lipopeptide	Antimicrobial peptide	Small molecule	Small molecule	Dendrimer
Antibacterial spectrum	G$^+$	G$^+$ and G$^-$	G$^+$	G$^+$	Certain G$^-$
Interacting lipid species	PG and CL	PG and CL	PE, PG, and CL	PG and CL	PG and CL
Stoichiometric ratio (drug/PG)	1.00	0.44	0.95	1.04	0.049
Binding affinity (M)	3.10×10^{-6}	5.76×10^{-7}	4.04×10^{-5}	4.45×10^{-6}	3.51×10^{-9}
Cytotoxicity	0.50 g of doses caused 20–40% cell lysis	IC$_{50}$ > 80 μM	IC$_{50}$ of AMG = 20 and IBC = 156 μM	IC$_{50}$ = 10 μM	IC$_{50}$ > 100 μM
Reference	(47, 48, 74)	(31)	(30, 75, 76)	This study and (77)	This study and (19)

bacterial strains may be the possible cause. For example, *K. pneumoniae* has been observed to exhibit a varied PG distribution (5 to 35%) under certain conditions (49, 50). This may explain the different MIC values of **AD1b** in different strains of *K. pneumoniae* (Fig. 1B). The zwitterionic phospholipid PC, absent in *E. coli*, has been found in the membranes of *P. aeruginosa* and *K. pneumoniae* with distribution ratios of 4.0 and 14.5%, respectively (49, 51, 52). These findings may also explain why PG-targeting **AD1b** shows different activity levels dependent on the Gram-negative bacterial strain tested.

Notably, the selective antibacterial activity spectrum of **AD1b** can be further exploited to design narrow-spectrum antibiotics that target only specific groups of bacteria without increasing the risk of developing antibiotic resistance in other bacteria because broad-spectrum antibiotics generate drug resistance and often harm beneficial microbial communities inhabiting humans (53). Narrowing the spectrum of antibacterial agents now appears to represent a feasible perspective for precision antibacterial therapies to combat AMR.

Last, amphiphilic dendrimers can self-assemble into nanostructures that accommodate drug molecules for combination therapy and harness the advantages of nanotechnology-based drug delivery for specific accumulation at the site of infection and inflammation (54–57). Such an approach offers a future perspective combining nanotechnology-based delivery of antibacterial agents with antibiotics for greater specificity and efficacious treatment of drug-resistant bacterial infections. We are actively pursuing this avenue of research.

MATERIALS AND METHODS
Materials and reagents
AD1b was synthesized as previously reported (19). The bacterial strains used in this project are listed in table S1. All antibiotics were purchased from Sigma-Aldrich. Dendrimers were synthesized by the previous protocol (58). LB (catalog no. 244620) was purchased from Becton Dickinson.

Bacterial growth conditions
For most experiments, one single bacterial colony was picked and cultured overnight using 2.0 ml of LB in a 15-ml round-bottom centrifuge tube (Axygen) at 37°C and 220 rpm. Overnight cultures were diluted 1:100 into 25 ml of fresh LB and grown for about 2.0 hours to the optical density at 600 nm (OD$_{600}$) = 0.40 to 0.50, which

corresponds to a bacterial density of about 10^8 colony-forming units (CFU) ml^{-1}. OD$_{600}$ measurements were performed using a Spectra-Max M5 microplate reader (Molecular Devices) and polystyrene cuvette (ISOLAB) with 1.0 ml of bacterial culture.

Antibacterial tests
MIC determination was performed according to the previous study (31). Briefly, dendrimers or other antibiotics were twofold diluted in LB broth and mixed with an equal volume of bacterial suspensions in LB containing approximately 1.5×10^6 CFU ml^{-1} in a clear, ultraviolet-sterilized, 96-well microtiter plate (Corning). OD$_{600}$ measurements were performed after incubation at 37°C for 18 hours. The MICs were defined as the lowest concentrations of dendrimer or antibiotics with no visible growth of bacteria.

Bacterial killing assays
Bacterial killing assays were performed according to the previous study (59). Briefly, the bacterial strains were cultured at OD$_{600}$ = 0.45 in LB as previously described, the bacterial density being approximately 4.0×10^8 CFU ml^{-1}. **AD1b** and antibiotic treatments were performed as indicated. At each time point, 1.0 ml of bacterial culture was acquired and washed twice with filtered 1× PBS (pH 7.2) (Santa Cruz Biotechnology) to remove the drugs. Washed bacterial cultures were then serially diluted in 1× PBS on a 96-well plate and 5.0 μl of each dilution was plated onto LB-agar plates to determine viable bacteria after overnight incubation at 37°C. Measurements were carried out in triplicate, and the following formula: [(colonies) × (dilution factor)] / (volume plated in milliliters) was used to calculate CFU ml^{-1} values. Mean CFU per millimeter values and SD were calculated for each treatment.

Resistance development assay
The resistance development assay was performed as previously described (60). Briefly, exponentially growing *E. coli* MG1655 and *A. baumannii* ATCC 17978 were diluted 1:100, resulting in a bacterial concentration of approximately 10^6 CFU ml^{-1}. This solution was then placed in 2.0-ml EP tubes containing 1.0 ml of LB, along with various concentrations (0.25, 0.50, 1.0, 2.0, and 4.0 × MIC) of **AD1b** or norfloxacin, the control antibiotics. Bacteria were incubated at 37°C and 220 rpm and passaged every 24 hours. Cultures from the highest concentration that allowed growth were diluted 1:100 into the fresh media with various concentrations

(0.25, 0.50, 1.0, 2.0, and 4.0 × MIC) of the respective drug. When MIC levels increased, concentrations of the respective antimicrobial were adjusted for next passaging. Serial passaging was repeated for 30 days, and the MIC changes were measured by dividing the respective daily MICs by the MIC on day 1.

PrestoBlue assay

RAW267.4, NIH 3T3, CHO K1, and Vero cells were seeded at 4.0×10^3 cells per well at 50 μl per well in 96-well plates and allowed to grow overnight. Cells were then treated with 50 μl of **AD1b** at various concentrations (1.69 to 217 μg ml^{-1}) and incubated for 48 hours (37° ± 0.5°C, 5% CO$_2$, and 95% humidity). Then, 10 μl of PrestoBlue reagent was added to each well containing 100 μl of blank, control, or treated cells in culture and incubated for another 1 to 3 hours at 37°C. Cell viability was detected by fluorescence spectroscopy (excitation wavelength λ_{ex} = 570 nm; emission wavelength λ_{em} = 610 nm). Cell viability was expressed as a percentage relative to untreated cells. All tests were run in triplicate.

LDH release assay

RAW264.7, NIH 3T3, CHO K1, and Vero cells were seeded at 4.0×10^3 cells per well in 96-well plates at 50 μl per well and allowed to grow overnight. Cells were then treated with 50 μl of **AD1b** at various concentrations (1.69 to 217 μg ml^{-1}) and incubated for 48 hours. Cell membrane damage was determined using the CytoTox-ONE Homogeneous Membrane Integrity Assay (Promega). The LDH reaction mixture was freshly prepared according to the manufacturer's protocol, and 50 μl was added to each well of a fresh round-bottom 96-well plate containing 50 μl of blank, control, or treated cells. The plates were incubated for 30 min at room temperature, followed by the addition of 50 μl of Stop solution provided by the manufacturer. Fluorescence was measured at 490 nm by fluorescence spectroscopy. Positive and negative controls were performed with lysis buffer and medium and set as 100 and 0% LDH release, respectively. Each assay was performed in triplicate. LDH% = [(the absorbance of sample − the absorbance of negative control) / (the absorbance of positive control − the absorbance of negative control)] × 100%.

Hemolytic activity

The hemolytic activity of dendrimer and colistin was measured as previously described previously (*19*, *61*). In summary, sterile defibrinated sheep blood cells were washed with filtered 1× PBS until no color was observed in the supernatant. A total of 1.0 ml of 8% sheep blood cells were treated with different concentrations of **AD1b** (0 to 256 μg ml^{-1}) or colistin (0 to 256 μg ml^{-1}) at 37°C for 1.0 hour to determine hemolytic activity. Triton X-100 (0.2%) and PBS were used as positive and negative controls, respectively. After incubation, cells were centrifuged at 6000 rpm for 10 min. Supernatant (200 μl) was collected and added to a 96-well plate to analyze hemoglobin absorbance at 576 nm using a SpectraMax M5 microplate reader. The hemolysis rate was determined using the formula described previously (*61*).

Scanning electron microscopy

SEM studies were performed by Wuhan Maisp Biotechnology Co. Ltd. Briefly, overnight cultured *E. coli* MG1655 was diluted 1:100 in fresh LB medium and grown at 37°C and 220 rpm until OD$_{600}$ = 0.45 to 0.50, which corresponds to a bacterial density of approximately 10^8 CFU ml^{-1}. The cultures were treated with **AD1b** and antibiotic control as specified for 1.5 hours. Subsequently, the bacteria were harvested by centrifugation at 4000 rpm for 10 min and washed twice with 1× PBS. The drug-treated samples were fixed in 2.5% glutaraldehyde (pH 7.4) overnight. Following three washes with 0.10 M phosphate buffer (pH 7.2), the samples were fixed in 1% osmic acid at 4°C for 2.0 hours. The samples were then dehydrated with a series of graded ethanol solutions, subjected to replacement with isoamyl acetate and critical point–dried. Last, samples were sputter-coated with gold for 30 s and observed with a Hitachi Regulus 8100 SEM.

Membrane integrity assay

Overnight bacterial cultures were washed twice and resuspended in filtered 1× PBS at an OD$_{600}$ of 0.45 to 0.50, which bacterial density is approximately 10^8 CFU ml^{-1}. The cultures were then stained with PI (1.0 μg ml^{-1}; Thermo Fisher Scientific, P1304MP) for 10 min. PI-labeled bacterial cells (190 μl) were added to each well of a black 96-well plate (Greiner). Then, 10 μl of PBS, **AD1b,** or positive control colistin was added, and the fluorescence intensity was measured at 37°C for 30 min with a Cytation 3 microplate reader (BioTek) with excitation and emission wavelengths of 535 and 617 nm, respectively.

Effect of lipids on the antibacterial activity of dendrimers

PC (Sigma-Aldrich, catalog no. 840051P), PE (Sigma-Aldrich, 840027P), PG (Sigma-Aldrich, catalog no. 841188P), CL (Sigma-Aldrich, 841199P), PGN (Sigma-Aldrich, catalog no. 77140), and LPS (Sigma-Aldrich, catalog no. L2630) were purchased from Sigma-Aldrich and dissolved as previously described (*31*). Checkerboard assays were performed as previously described (*30*). Briefly, **AD1b** was subjected to a twofold dilution with 100 μl of LB medium along the abscissa of a 96-well plate. Bacterial strains were cultured at an OD$_{600}$ = 0.40 and diluted as previously reported. One hundred microliters of the diluted bacterial suspension (approximately 1.5×10^6 CFU ml^{-1}) containing varying concentrations of lipids (0 to 128 μg ml^{-1}) was added to each well of the 96-well plate containing the same volume of dendrimers. OD600 measurement and MIC determination were performed according to the experimental procedures detailed in the "Antibacterial tests" section.

Computational methods

A symmetric lipid bilayer composed of 239 lipids per leaflet with ratio 70:20:10 of 1-palmitoyl-2-oleoyl-*sn*-glycero-3-phosphoethanolamine (POPE), 1-palmitoyl-2-oleoyl-*sn*-glycero-3-phosphoglycerol (POPG), and CL (with symmetric 1-palmitoyl-2-oleoyl tails) was built using packmol-memgen (*62*) provided by the AMBER 22 (*63*) suite of programs. Explicit transferable intermolecular potential with three points (TIP3P) (*64*) water molecules were added to reach complete membrane hydration and to allow placement of **AD1b** monomers above the lipid surface. Sodium and chlorine ions were added to achieve charge neutrality. The **AD1b** monomer was parameterized with the same protocol described in our previous work (*65*), briefly based on gaff2 (*66*) atom types and partial charges derived using the restrained electrostatic potential (RESP) method offered by the R.E.D. server (*67*). The lipid21 force field (*68*) was used to parameterize the lipids. The membrane and membrane-**AD1b** systems were subjected to a well-established simulation protocol, as discussed in detail in our previous work (*19*). Data collection for **AD1b** in complex with each of the studied lipids was carried out for

1 µs, in the isothermal-isobaric ensemble (NPT ensemble). Where a stable complex was obtained, 100 frames from the last 300 ns of data collection were extracted to be analyzed in the framework of the MM/PBSA ansatz (*69*) implemented in MMPBSA.py (*36*). The internal dielectric constant was set to 8 to account for the presence of the charged environment at the binding interface.

The model for the outer membrane of Gram-negative bacteria was built via the CHARMM-GUI web server (*70*), where the outer leaflet was composed 100% of LPS, for which the deep rough mutant lipopolysaccharide (RaLPS) model was selected, and the inner leaflet was composed of 80% POPE, 10% POPG, and 10% CL, with a size of 76 Å by 76 Å. Calcium and sodium ions were used to neutralize the systems. To perform umbrella sampling simulations, the position, along the perpendicular direction to the membrane (Z), of the center of mass of **AD1b** was restrained at 1-Å intervals, with a force constant of 3 kcal mol^{-1} Å^{-2}. Each window was simulated for 500 ns to collect the relevant data. The weighted histogram analysis method was used to retrieve the final free energy profile (*71*). All simulation studies were carried out in AMBER 22 (*63*) running on our own graphics processing unit/central processing unit hybrid cluster and in the Marconi-100 high-performance facility offered by the Italian CINECA.

ITC assay

The interaction between **AD1b** and PG, PC, and PE was first evaluated by a MicroCal ITC assay (Malvern Panalytical) at 25°C using the one set of sites binding model. **AD1b** (50 µM) dissolved in 20 mM Hepes buffer (pH 7.0) was sequentially injected into calorimetric cells filled with 100 µM PG, PC, or PE dissolved in the same buffer. BMS (300 µM; dissolved in 20 mM Hepes buffer) was sequentially injected into the calorimetric cells containing 40 µM PG. All injections were repeated 20 times at an equilibrium interval of 150 s. The results were processed using the instrument software to calculate the equilibrium dissociation constant (K_D), stoichiometry (n), and changes in enthalpy (ΔH) and entropy (ΔS). The experimental procedures were carried out in triplicate, and the resulting values of the relevant parameters were averaged to obtain the data used for the competitive ITC assay. The measured binding enthalpies and binding constant of BMS and PG in this article are as follows: $\Delta H = -7.94$ kcal mol^{-1}, $K_B = 2.44 \times 10^5$ M, and $n = 1.04$. The competitive ITC assay was performed according to a previous study (*38*). **AD1b** (50 µM) was sequentially injected into the calorimetric cells containing the mixed solution of 100 µM PG and 10 µM BMS at 25°C. All injections were repeated 20 times at an equilibrium interval of 150 s. The results were processed using a competitive binding model in the instrument software, and the experiments were conducted in triplicate.

Membrane depolarization assay

Membrane depolarization assays were performed as previously described (*72*). Briefly, overnight bacterial cultures were washed twice and resuspended in filtered 1× PBS at an OD$_{600}$ of 0.45 to 0.50, which bacterial density is approximately 10^8 CFU ml^{-1}. The cultures were then stained with 1 µM DiSC$_3$(5) (Thermo Fisher Scientific) at 37°C for 10 min. Labeled bacterial cells (190 µl) were added to a black 96-well plate (Greiner). Subsequently, 10 µl of **AD1b** and the positive control, valinomycin (5.0 µM), were added. Fluorescence intensity was measured at 37°C for 30 min using the Cytation 3 microplate reader (BioTek) at excitation and emission wavelengths of 622 and 670 nm, respectively.

ΔpH measurements

ΔpH measurements were performed according to the previous study (*30*). Briefly, overnight bacterial cultures were washed twice with Hepes buffer [5.0 mM (pH 7.0) plus 5.0 mM glucose) and adjusted to an OD$_{600}$ of 0.45 to 0.50, which bacterial density is about 10^8 CFU ml^{-1}. The cultures were then stained with 5.0 µM BCECF-AM (Thermo Fisher Scientific) at 37°C for 10 min, and 190 µl of stained cells were added to a black 96-well plate. Subsequently, 10 µl of **AD1b** was added as indicated concentrations. The fluorescence intensity was measured at 37°C for 30 min using the Cytation 3 microplate reader (BioTek) at excitation and emission wavelengths of 488 and 535 nm, respectively.

INT reduction assay

The INT reduction assay was performed as previously described with a minor modification (*32*). Briefly, overnight bacterial cultures were washed twice and resuspended in 0.1 M potassium phosphate buffer (pH 7.5) at an OD$_{600}$ of 0.45 to 0.50, which bacterial density is about 10^8 CFU ml^{-1}. The cultures were then stained with 1 mM INT. Then, different concentrations of **AD1b** and a positive control antibiotic, colistin (16 µg ml^{-1}), were added. Samples (200 µl) were transferred to a 96-well plate, and absorbance at 490 nm was measured at 37°C for 1.0 hour with 10-min intervals.

ATP measurement

ATP measurements were made using the BacTiter-Glo Microbial Cell Viability Assay Kit (Promega). Briefly, overnight bacterial cultures were washed twice and resuspended in filtered 1× PBS at an OD$_{600}$ of 0.45 to 0.50, which bacterial density is approximately 10^8 CFU ml^{-1}. Dendrimer and antibiotic treatments were administered as indicated for a duration of 1.5 hours. Subsequently, the drug-treated bacteria were subjected to centrifugation at 12,000 rpm for 5 min. The resulting supernatants were again centrifuged and collected to determine the level of extracellular ATP. The precipitates were resuspended in the same volume of PBS to assess the intracellular ATP level. Bacterial samples (100 µl) were added to a black 96-well plate, followed by the addition of the BacTiter-Glo reagent (100 µl) to each well. After 5-min incubation at room temperature, ATP levels were measured using a SpectraMax M5 microplate reader (Molecular Devices) in the luminescence mode.

Determination of extracellular protein concentrations

Extracellular protein concentrations were determined with slight modifications to the method previously described (*73*). Briefly, bacterial cultures were grown overnight, washed twice, and resuspended in filtered 1× PBS at an OD$_{600}$ of 0.45 to 0.50, which bacterial density is approximately 10^8 CFU ml^{-1}. Dendrimer and antibiotic treatments were administered as indicated for 3.0 hours. Subsequently, the bacterial cultures were subjected to centrifugation at 8000 rpm for 10 min, and the resulting supernatants were collected to measure the extracellular protein concentration using a bicinchoninic acid protein assay kit (Pierce).

ROS determination

Overnight bacterial cultures were washed twice and resuspended in filtered 1× PBS at an OD$_{600}$ of 0.45 to 0.50, which bacterial density is about 10^8 CFU ml^{-1}. The cultures were then stained with carboxy-H2DCFDA (10 µM) at 37°C for 30 min. After washing with 1× PBS twice, the probe-labeled bacterial cells (190 µl) were added to a black

96-well plate (Greiner). Subsequently, 10 μl of **AD1b** and the positive control, colistin (8.0 μg ml^{-1}), were added. After incubating at 37°C for 1.5 hours, fluorescence intensity was measured using the Cytation 3 microplate reader (BioTek) at excitation and emission wavelengths of 488 and 525 nm, respectively.

Encapsulation of Cy7.5 into AD1b nanomicelles for biodistribution study
For live in vivo live imaging of **AD1b** biostability and biodistribution, we encapsulated the hydrophobic Cy7.5 in the **AD1b** nanomicelles using the film dispersion method. **AD1b** and Cy7.5 were mixed in 3:0.1 (w/w) ratio in CHCl$_3$:MeOH mixed solvent (3:1, v/v) and then evaporated on a rotary evaporator until a clear film appeared after removal of organic solvents. The thin film was dispersed in PBS buffer and vortexed for 10 min or until a clear solution was obtained. This solution was filtered through a 0.22 μm sterile filter. Fluorescence spectroscopic analysis was used to quantify encapsulated Cy7.5 in dendrimer nanomicelles using a fluorescence spectrophotometer with excitation and emission wavelengths of 788 and 808 nm, respectively. The encapsulation efficiency of Cy7.5 was found to be 94%.

Ethics statement
Animal experiments were carried out strictly following the guidelines described in the Guide for the Care and Use of Laboratory Animals of the US National Institutes of Health. The animal protocols were reviewed and approved by the University of Illinois at Urbana-Champaign Institutional Animal Care and Use Committee (no. 22051) and by the Animal Research Ethics Committee of the University of Macau (UMARE-016-2022). Six-week-old CD-1 mice (males and females) were purchased from Charles River Laboratories (Wilmington, MA, USA). The mice were acclimated for 1 week before experimentation. All mice were provided food, water, and bedding and housed in positively ventilated microisolator cages with automatic recirculating water located in a room with laminar, high-efficiency particulate-filtered air.

In vivo imaging of AD1b pharmacokinetics
Both biostability and biodistribution of **AD1b** were determined by live in vivo imaging with an IVIS SpectrumCT imaging system (PerkinElmer, Waltham, MA, USA). CD-1 mice (groups of four) were anesthetized with 3% isoflurane, administered 50 μg of Cy7.5-**AD1b**, and imaged with the following settings: binning factor = 1, f number = 1, field of view = 25.4, and fluorescence exposure time for 60 s. The images were analyzed using Living Image software (PerkinElmer).

Toxicity studies of AD1b
CD-1 mice (groups of five) were injected intraperitoneally twice daily with **AD1b** (5 mg kg^{-1}) or sterile saline control (in 50 μl) for 7 days. Mouse weight was determined once a day, and the animals were euthanized on the eighth day. The main organs, including the livers, lungs, kidneys, hearts, and spleens, were harvested, fixed in 10% neutral buffered formalin for 24 hours, embedded in paraffin, and sectioned and stained with hematoxylin and eosin. Stain organ tissues were imaged using an Olympus DP70 light microscope and analyzed in a double-blind manner by an anatomic pathologist at the University of Illinois at Urbana-Champaign Veterinary Diagnostic Laboratory (Olympus, Central Valley, PA, USA).

Mouse models of acute pneumonia and bacteremia
For the acute pneumonia model of lung infection, CD-1 mice ($n = 8$ per group) were intranasally inoculated with 3.8×10^8 CFU of *E. coli* AR Bank 0349 or 2.0×10^8 CFU of *A. baumannii* W49717. For bacteremia, CD-1 mice ($n = 6$ per group) were infected intraperitoneally with 7.8×10^7 CFU of *E. coli* AR Bank 0349 or 5.3×10^7 CFU of *A. baumannii* W49717. Infected mice were treated by intraperitoneal injection of **AD1b** (5 mg kg^{-1}) twice daily or with the same volume of sterile PBS in the control groups. Infected lungs and spleens were harvested at 48 and 24 hpi, respectively, and homogenized in 1 ml of sterile PBS using the Omni Soft Tissue Tip Homogenizer (Genizer LLC, Irvine, CA, USA). The bacterial burden was determined after serial dilution plating of the homogenates in LB agar plates.

Mouse model of sepsis mortality
CD-1 mice ($n = 15$ per group) were infected intravenously with 4.3×10^8 CFU of *E. coli* AR Bank 0349 or 2.5×10^8 CFU of *A. baumannii* W49717 by intraperitoneal route. Mice were treated twice daily with **AD1b** (5 mg kg^{-1}) intraperitoneally, beginning at 2 hpi. Mice in control groups were administered the same volume of sterile PBS. Mouse mortality was monitored for 144 hours.

Statistical analysis
Statistical analysis was performed using GraphPad Prism software. The unpaired Student's *t* test method or one-way analysis of variance (ANOVA) was used to determine statistical significance. A *P* value less than 0.05 was considered significant (*$P < 0.05$, **$P < 0.01$, ***$P < 0.001$, and ****$P < 0.0001$). Mouse survival studies were analyzed with the Kaplan-Meier log rank survival test using the GraphPad Prism.

Supplementary Materials
This PDF file includes:
Tables S1 to S5
Figs. S1 to S8
References

REFERENCES AND NOTES
1. K. Kupferschmidt, Resistance fighters. *Science* **352**, 758–761 (2016).
2. A. H. Holmes, L. S. Moore, A. Sundsfjord, M. Steinbakk, S. Regmi, A. Karkey, P. J. Guerin, L. J. Piddock, Understanding the mechanisms and drivers of antimicrobial resistance. *Lancet* **387**, 176–187 (2016).
3. J. Davies, D. Davies, Origins and evolution of antibiotic resistance. *Microbiol. Mol. Biol. Rev.* **74**, 417–433 (2010).
4. D. M. P. De Oliveira, B. M. Forde, T. J. Kidd, P. N. A. Harris, M. A. Schembri, S. A. Beatson, D. L. Paterson, M. J. Walker, Antimicrobial resistance in ESKAPE pathogens. *Clin. Microbiol. Rev.* **33**, e00181–19 (2020).
5. J. Denissen, B. Reyneke, M. Waso-Reyneke, B. Havenga, T. Barnard, S. Khan, W. Khan, Prevalence of ESKAPE pathogens in the environment: Antibiotic resistance status, community-acquired infection and risk to human health. *Int. J. Hyg. Envir. Heal* **244**, 114006 (2022).
6. Antimicrobial Resistance Collaborators, Global burden of bacterial antimicrobial resistance in 2019: A systematic analysis. *Lancet* **399**, 629–655 (2022).
7. J. M. Blair, M. A. Webber, A. J. Baylay, D. O. Ogbolu, L. J. V. Piddock, Molecular mechanisms of antibiotic resistance. *Nat. Rev. Microbiol.* **13**, 42–51 (2015).
8. S. Hernando-Amado, T. M. Coque, F. Baquero, J. L. Martinez, Defining and combating antibiotic resistance from One Health and Global Health perspectives. *Nat. Microbiol.* **4**, 1432–1442 (2019).
9. E. M. Darby, E. Trampari, P. Siasat, M. S. Gaya, I. Alav, M. A. Webber, J. M. A. Blair, Molecular mechanisms of antibiotic resistance revisited. *Nat. Rev. Microbiol.* **21**, 280–295 (2023).
10. D. G. J. Larsson, C. F. Flach, Antibiotic resistance in the environment. *Nat. Rev. Microbiol.* **20**, 257–269 (2022).

11. C. Ardal, M. Balasegaram, R. Laxminarayan, D. McAdams, K. Outterson, J. H. Rex, N. Sumpradit, Antibiotic development - Economic, regulatory and societal challenges. *Nat. Rev. Microbiol.* **18**, 267–274 (2020).

12. M. Miethke, M. Pieroni, T. Weber, M. Brönstrup, P. Hammann, L. Halby, P. B. Arimondo, P. Glaser, B. Aigle, H. B. Bode, R. Moreira, Y. N. Li, A. Luzhetskyy, M. H. Medema, J. L. Pernodet, M. Stadler, J. R. Tormo, O. Genilloud, A. W. Truman, K. J. Weissman, E. Takano, S. Sabatini, E. Stegmann, H. Brötz-Oesterhelt, W. Wohlleben, M. Seemann, M. Empting, A. K. H. Hirsch, B. Loretz, C. M. Lehr, A. Titz, J. Herrmann, T. Jaeger, S. Alt, T. Hesterkamp, M. Winterhalter, A. Schiefer, K. Pfarr, A. Hoerauf, H. Graz, M. Graz, M. Lindvall, S. Ramurthy, A. Karlén, M. van, H. Petkovic, A. Keller, F. Peyrane, S. Donadio, L. Fraisse, L. J. V. Piddock, I. H. Gilbert, H. E. Moser, R. Müller, Towards the sustainable discovery and development of new antibiotics. *Nat. Rev. Chem.* **5**, 726–749 (2021).

13. T. J. Hall, V. M. Villapun, O. Addison, M. A. Webber, M. Lowther, S. E. T. Louth, S. E. Mountcastle, M. Y. Brunet, S. C. Cox, A call for action to the biomaterial community to tackle antimicrobial resistance. *Biomater. Sci.* **8**, 4951–4974 (2020).

14. R. Y. K. Chang, S. C. Nang, H. K. Chan, J. Li, Novel antimicrobial agents for combating antibiotic-resistant bacteria. *Adv. Drug Deliv. Rev.* **187**, 114378 (2022).

15. A. R. Kirtane, M. Verma, P. Karandikar, J. Furin, R. Langer, G. Traverso, Nanotechnology approaches for global infectious diseases. *Nat. Nanotechnol.* **16**, 369–384 (2021).

16. S. J. Lam, N. M. O'Brien-Simpson, N. Pantarat, A. Sulistio, E. H. Wong, Y. Y. Chen, J. C. Lenzo, J. A. Holden, A. Blencowe, E. C. Reynolds, G. G. Qiao, Combating multidrug-resistant Gram-negative bacteria with structurally nanoengineered antimicrobial peptide polymers. *Nat. Microbiol.* **1**, 16162 (2016).

17. T. N. Siriwardena, M. Stach, R. Z. He, B. H. Gan, S. Javor, M. Heitz, L. Ma, X. J. Cai, P. Chen, D. W. Wei, H. T. Li, J. Ma, T. Köhler, C. van, T. Darbre, J. L. Reymond, Lipidated peptide dendrimers killing multidrug-resistant bacteria. *J. Am. Chem. Soc.* **140**, 423–432 (2018).

18. Z. Lai, Q. Jian, G. Li, C. Shao, Y. Zhu, X. Yuan, H. Chen, A. Shan, Self-assembling peptide dendron nanoparticles with high stability and a multimodal antimicrobial mechanism of action. *ACS Nano* **15**, 15824–15840 (2021).

19. D. Dhumal, B. Maron, E. Malach, Z. B. Lyu, L. Ding, D. Marson, E. Laurini, A. Tintaru, B. Ralahy, S. Giorgio, S. Pricl, Z. Hayouka, L. Peng, Dynamic self-assembling supramolecular dendrimer nanosystems as potent antibacterial candidates against drug-resistant bacteria and biofilms. *Nanoscale* **14**, 9286–9296 (2022).

20. C. Galanakou, D. Dhumal, L. Peng, Amphiphilic dendrimers against antibiotic resistance: Light at the end of the tunnel? *Biomater. Sci.* **11**, 3379–3393 (2023).

21. A. Castonguay, E. Ladd, T. G. M. van de Ven, A. Kakkar, Dendrimers as bactericides. *New J. Chem.* **36**, 199–204 (2012).

22. M. A. Mintzer, E. L. Dane, G. O'Toole, M. W. Grinstaff, Exploiting dendrimer multivalency to combat emerging and re-emerging infectious diseases. *Mol. Pharm.* **9**, 342–354 (2012).

23. C. C. Lee, J. A. MacKay, J. M. J. Frechet, F. C. Szoka, Designing dendrimers for biological applications. *Nat. Biotechnol.* **23**, 1517–1526 (2005).

24. Z. W. Zhou, M. Cong, M. Y. Li, A. Tintaru, J. Li, J. H. Yao, Y. Xia, L. Peng, Negative dendritic effect on enzymatic hydrolysis of dendrimer conjugates. *Chem. Commun.* **54**, 5956–5959 (2018).

25. N. King, D. Dhumal, S. Q. Lew, S. H. Kuo, C. Galanakou, M. W. Oh, S. Y. Chong, N. Zhang, L. T. O. Lee, Z. Hayouka, L. Peng, G. W. Lau, Amphiphilic dendrimer as potent antibacterial against drug-resistant bacteria in mouse models of human infectious diseases. *ACS Infect. Dis.* **10**, 453–466 (2024).

26. J. M. Cisneros, J. Rodriguez-Bano, Nosocomial bacteremia due to *Acinetobacter baumannii*: Epidemiology, clinical features and treatment. *Clin. Microbiol. Infec.* **8**, 687–693 (2002).

27. J. Vila, E. Saez-Lopez, J. R. Johnson, U. Romling, U. Dobrindt, R. Canton, C. G. Giske, T. Naas, A. Carattoli, M. Martinez-Medina, J. Bosch, P. Retamar, J. Rodriguez-Bano, F. Baquero, S. M. Soto, *Escherichia coli*: An old friend with new tidings. *FEMS Microbiol. Rev.* **40**, 437–463 (2016).

28. J. Vila, J. Moreno-Morales, C. Balleste-Delpierre, Current landscape in the discovery of novel antibacterial agents. *Clin. Microbiol. Infect.* **26**, 596–603 (2020).

29. R. M. Epand, C. Walker, R. F. Epand, N. A. Magarvey, Molecular mechanisms of membrane targeting antibiotics. *Biochim. Biophys. Acta* **1858**, 980–987 (2016).

30. M. Song, Y. Liu, T. Li, X. Liu, Z. Hao, S. Ding, P. Panichayupakaranant, K. Zhu, J. Shen, Plant natural flavonoids against multidrug resistant pathogens. *Adv. Sci.* **8**, e2100749 (2021).

31. M. Song, Y. Liu, X. Huang, S. Ding, Y. Wang, J. Shen, K. Zhu, A broad-spectrum antibiotic adjuvant reverses multidrug-resistant Gram-negative pathogens. *Nat. Microbiol.* **5**, 1040–1050 (2020).

32. M. A. Farha, C. P. Verschoor, D. Bowdish, E. D. Brown, Collapsing the proton motive force to identify synergistic combinations against *Staphylococcus aureus*. *Chem. Biol.* **20**, 1168–1178 (2013).

33. S. A. Anuj, H. P. Gajera, D. G. Hirpara, B. A. Golakiya, Bacterial membrane destabilization with cationic particles of nano-silver to combat efflux-mediated antibiotic resistance in Gram-negative bacteria. *Life Sci.* **230**, 178–187 (2019).

34. M. A. Lobritz, P. Belenky, C. B. M. Porter, A. Gutierrez, J. H. Yang, E. G. Schwarz, D. J. Dwyer, A. S. Khalil, J. J. Collins, Antibiotic efficacy is linked to bacterial cellular respiration. *Proc. Natl. Acad. Sci. U. S. A.* **112**, 8173–8180 (2015).

35. M. A. Kohanski, D. J. Dwyer, B. Hayete, C. A. Lawrence, J. J. Collins, A common mechanism of cellular death induced by bactericidal antibiotics. *Cell* **130**, 797–810 (2007).

36. B. R. Miller III, T. McGee Jr., J. Swails, N. Homeyer, H. Gohlke, A. E. Roitberg, MMPBSA.py: An efficient program for end-state free energy calculations. *J. Chem. Theory. Comput.* **8**, 3314–3321 (2012).

37. M. Schlame, Cardiolipin synthesis for the assembly of bacterial and mitochondrial membranes. *J. Lipid Res.* **49**, 1607–1620 (2008).

38. H. Ohtaka, A. Velazquez-Campoy, D. Xie, E. Freire, Overcoming drug resistance in HIV-1 chemotherapy: The binding thermodynamics of Amprenavir and TMC-126 to wild-type and drug-resistant mutants of the HIV-1 protease. *Protein Sci.* **11**, 1908–1916 (2002).

39. N. Zhang, W. Shan, L. Gao, S. H. Kou, C. Lu, H. Yang, B. Peng, K. Y. Tam, L. T. O. Lee, J. Zheng, Repurposing the Hedgehog pathway inhibitor, BMS-833923, as a phosphatidylglycerol-selective membrane-disruptive colistin adjuvant against ESKAPE pathogens. *Int. J. Antimicrob. Agents* **62**, 106888 (2023).

40. K. L. Stuart, S. M. Shore, T. L. Nicholson, Complete genome sequence of escherichia coli antibiotic-resistant isolate AR bank #0349. *Microbiol. Resour. Announc.* **8**, e01078–19 (2019).

41. H. E. Caraway, J. Z. Lau, B. Maron, M. W. Oh, Y. Belo, A. Brill, E. Malach, N. Ismail, Z. Hayouka, G. W. Lau, Antimicrobial random peptide mixtures eradicate *Acinetobacter baumannii* biofilms and inhibit mouse models of infection. *Antibiotics* **11**, 413 (2022).

42. E. N. Parker, B. S. Drown, E. J. Geddes, H. Y. Lee, N. Ismail, G. W. Lau, P. J. Hergenrother, Implementation of permeation rules leads to a FabI inhibitor with activity against Gram-negative pathogens. *Nat. Microbiol.* **5**, 67–75 (2020).

43. D. Mehta, V. Saini, B. Aggarwal, A. Khan, A. Bajaj, Unlocking the bacterial membrane as a therapeutic target for next-generation antimicrobial amphiphiles. *Mol. Aspects Med.* **81**, 100999 (2021).

44. W. Dowhan, Molecular basis for membrane phospholipid diversity: Why are there so many lipids? *Annu. Rev. Biochem.* **66**, 199–232 (1997).

45. J. E. Vance, Phospholipid synthesis and transport in mammalian cells. *Traffic* **16**, 1–18 (2015).

46. C. Fenton, G. M. Keating, M. P. Curran, Daptomycin. *Drugs* **64**, 445–455 (2004).

47. S. Kilinc, T. Tunc, O. Pazarci, Z. Sumer, Research into biocompatibility and cytotoxicity of daptomycin, gentamicin, vancomycin and teicoplanin antibiotics at common doses added to bone cement. *Joint Dis. Relat. Surg.* **31**, 328–334 (2020).

48. S. D. Taylor, M. Palmer, The action mechanism of daptomycin. *Bioorg. Med. Chem.* **24**, 6253–6268 (2016).

49. M. K. Wassef, Lipids of *Klebsiella pneumoniae*: The presence of phosphatidyl choline in succinate-grown cells. *Lipids* **11**, 364–369 (1976).

50. K. L. F. Hilton, C. Manwani, J. E. Boles, L. J. White, S. Ozturk, M. D. Garrett, J. R. Hiscock, The phospholipid membrane compositions of bacterial cells, cancer cell lines and biological samples from cancer patients. *Chem. Sci.* **12**, 13273–13282 (2021).

51. P. J. Wilderman, A. I. Vasil, W. E. Martin, R. C. Murphy, M. L. Vasil, *Pseudomonas aeruginosa* synthesizes phosphatidylcholine by use of the phosphatidylcholine synthase pathway. *J. Bacteriol.* **184**, 4792–4799 (2002).

52. C. Sohlenkamp, O. Geiger, Bacterial membrane lipids: Diversity in structures and pathways. *FEMS Microbiol. Rev.* **40**, 133–159 (2016).

53. C. Carbon, R. Isturiz, Narrow versus broad spectrum antibacterials: Factors in the selection of pneumococcal resistance to β-lactams. *Drugs* **62**, 1289–1294 (2002).

54. Y. Jiang, Z. Lyu, B. Ralahy, J. Liu, T. Roussel, L. Ding, J. Tang, A. Kosta, S. Giorgio, R. Tomasini, X. J. Liang, N. Dusetti, J. Iovanna, L. Peng, Dendrimer nanosystems for adaptive tumor-assisted drug delivery via extracellular vesicle hijacking. *Proc. Natl. Acad. Sci. U.S.A.* **120**, e2215308120 (2023).

55. Z. Lyu, L. Ding, A. Tintaru, L. Peng, Self-assembling supramolecular dendrimers for biomedical applications: Lessons learned from poly(amidoamine) dendrimers. *Acc. Chem. Res.* **53**, 2936–2949 (2020).

56. T. Wei, C. Chen, J. Liu, C. Liu, P. Posocco, X. Liu, Q. Cheng, S. Huo, Z. Liang, M. Fermeglia, S. Pricl, X. J. Liang, P. Rocchi, L. Peng, Anticancer drug nanomicelles formed by self-assembling amphiphilic dendrimer to combat cancer drug resistance. *Proc. Natl. Acad. Sci. U.S.A.* **112**, 2978–2983 (2015).

57. Z. Lyu, B. Ralahy, T. A. Perles-Barbacaru, L. Ding, Y. Jiang, B. Lian, T. Roussel, X. Liu, C. Galanakou, E. Laurini, A. Tintaru, S. Giorgio, S. Pricl, X. Liu, M. Bernard, J. Iovanna, A. Viola, L. Peng, Self-assembling dendrimer nanosystems for specific fluorine magnetic resonance imaging and effective theranostic treatment of tumors. *Proc. Natl. Acad. Sci. U.S.A.* **121**, e2322403121 (2024).

58. T. Yu, X. Liu, A. L. Bolcato-Bellemin, Y. Wang, C. Liu, P. Erbacher, F. Qu, P. Rocchi, J. P. Behr, L. Peng, An amphiphilic dendrimer for effective delivery of small interfering RNA and gene silencing in vitro and in vivo. *Angew. Chem. Int. Ed. Engl.* **51**, 8478–8484 (2012).

59. X. Ji, J. Zou, H. Peng, A. S. Stolle, R. Xie, H. Zhang, B. Peng, J. J. Mekalanos, J. Zheng, Alarmone Ap4A is elevated by aminoglycoside antibiotics and enhances their bactericidal activity. *Proc. Natl. Acad. Sci. U.S.A.* **116**, 9578–9585 (2019).

60. P. Le, E. Kunold, R. Macsics, K. Rox, M. C. Jennings, I. Ugur, M. Reinecke, D. Chaves-Moreno, M. W. Hackl, C. Fetzer, F. A. M. Mandl, J. Lehmann, V. S. Korotkov, S. M. Hacker, B. Kuster, I. Antes, D. H. Pieper, M. Rohde, W. M. Wuest, E. Medina, S. A. Sieber, Repurposing human kinase inhibitors to create an antibiotic active against drug-resistant *Staphylococcus aureus*, persisters and biofilms. *Nat. Chem.* **12**, 145–158 (2020).

61. Y. Liu, Y. Jia, K. Yang, R. Li, X. Xiao, K. Zhu, Z. Wang, Metformin restores tetracyclines susceptibility against multidrug resistant bacteria. *Adv. Sci.* **7**, 1902227 (2020).

62. S. Schott-Verdugo, H. Gohlke, PACKMOL-Memgen: A simple-to-use, generalized workflow for membrane-protein-lipid-bilayer system building. *J. Chem. Inf. Model.* **59**, 2522–2528 (2019).

63. D. A. Case, H. M. Aktulga, K. Belfon, I. Y. Ben-Shalom, J. T. Berryman, S. R. Brozell, D. S. Cerutti, T. E. Cheatham III, G. A. Cisneros, V. W. D. Cruzeiro, T. A. Darden, R. E. Duke, G. Giambasu, M. K. Gilson, H. Gohlke, A. W. Goetz, R. Harris, S. Izadi, S. A. Izmailov, K. Kasavajhala, M. C. Kaymak, E. King, A. Kovalenko, T. Kurtzman, T. S. Lee, S. LeGrand, P. Li, C. Lin, J. Liu, T. Luchko, R. Luo, M. Machado, V. Man, M. Manathunga, K. M. Merz, Y. Miao, O. Mikhailovskii, G. Monard, H. Nguyen, K. A. O'Hearn, A. Onufriev, F. Pan, S. Pantano, R. Qi, A. Rahnamoun, D. R. Roe, A. Roitberg, C. Sagui, S. Schott-Verdugo, A. Shajan, J. Shen, C. L. Simmerling, N. R. Skrynnikov, J. Smith, J. Swails, R. C. Walker, J. Wang, J. Wang, H. Wei, R. M. Wolf, X. Wu, Y. Xiong, Y. Xue, D. M. York, S. Zhao, P. A. Kollman, *AMBER 2022* (University of California, 2022).

64. W. L. Jorgensen, J. Chandrasekhar, J. D. Madura, R. W. Impey, M. L. Klein, Comparison of simple potential functions for simulating liquid water. *J. Chem. Phys.* **79**, 926–935 (1983).

65. C. Chao, P. Paola, L. Xiaoxuan, C. Qiang, L. Erik, Z. Jiehua, L. Cheng, W. Yang, T. Jingjie, C. Valentina Dal, Y. Tianzhu, G. Suzanne, F. Maurizio, Q. Fanqi, L. Zicai, J. R. John, L. Minghua, R. Palma, P. Sabrina, P. Ling, siRNA delivery: Mastering dendrimer self-assembly for efficient siRNA delivery: From conceptual design to in vivo efficient gene silencing (Small 27/2016). *Small* **12**, 3604–3604 (2016).

66. J. Wang, R. Wolf, J. Caldwell, P. Kollman, D. Case, Development and testing of a general amber force field. *J. Comput. Chem.* **25**, 1157–1174 (2004).

67. E. Vanquelef, S. Simon, G. Marquant, E. Garcia, G. Klimerak, J. C. Delepine, P. Cieplak, F.-Y. Dupradeau, R.E.D. server: A web service for deriving RESP and ESP charges and building force field libraries for new molecules and molecular fragments. *Nucleic Acids Res.* **39**, W511–W517 (2011).

68. C. J. Dickson, R. C. Walker, I. R. Gould, Lipid21: Complex lipid membrane simulations with AMBER. *J. Chem. Theory. Comput.* **18**, 1726–1736 (2022).

69. E. Wang, H. Sun, J. Wang, Z. Wang, H. Liu, J. Z. H. Zhang, T. Hou, End-point binding free energy calculation with MM/PBSA and MM/GBSA: Strategies and applications in drug design. *Chem. Rev.* **119**, 9478–9508 (2019).

70. S. Jo, J. B. Lim, J. B. Klauda, W. Im, CHARMM-GUI membrane builder for mixed bilayers and its application to yeast membranes. *Biophys. J.* **97**, 50–58 (2009).

71. S. Kumar, D. Bouzida, R. H. Swendsen, P. A. Kollman, J. M. Rosenberg, The weighted histogram analysis method for free-energy calculations on biomolecules. I. The method. *J. Comput. Chem.* **13**, 1011–1021 (1992).

72. Y. Liu, Z. Tong, J. Shi, Y. Jia, T. Deng, Z. Wang, Reversion of antibiotic resistance in multidrug-resistant pathogens using non-antibiotic pharmaceutical benzydamine. *Commun. Biol.* **4**, 1328 (2021).

73. X. Song, T. Liu, L. Wang, L. Liu, X. Li, X. Wu, Antibacterial effects and mechanism of mandarin (*Citrus reticulata* L.) essential oil against *Staphylococcus aureus*. *Molecules* **25**, 4956 (2020).

74. R. Moreira, S. D. Taylor, Establishing the structure-activity relationship between phosphatidylglycerol and daptomycin. *ACS Infect. Dis.* **8**, 1674–1686 (2022).

75. X. F. Quan, Y. Wang, X. F. Ma, Y. Liang, W. X. Tian, Q. Y. Ma, H. Z. Jiang, Y. X. Zhao, α-Mangostin induces apoptosis and suppresses differentiation of 3T3-L1 cells via inhibiting fatty acid synthase. *PLOS ONE* **7**, e33376 (2012).

76. L. Zhao, Y. L. Yu, L. Li, J. R. Wang, J. Wang, S. J. Su, J. Y. Ding, Y. Zhang, A. H. Wang, K. Zhou, Isobavachalcone disrupts mitochondrial respiration and induces cytotoxicity through ROS accumulation and Akt suppression. *Toxicon* **216**, 28–36 (2022).

77. A. H. Zaidi, Y. Komatsu, L. A. Kelly, U. Malhotra, C. Rotoloni, J. E. Kosovec, H. Zahoor, R. Makielski, A. Bhatt, T. Hoppo, B. A. Jobe, Smoothened inhibition leads to decreased proliferation and induces apoptosis in esophageal adenocarcinoma cells. *Cancer Invest.* **31**, 480–489 (2013).

78. C. Lu, N. Zhang, S. Kou, L. Gao, B. Peng, Y. Dai, J. Zheng, Sanguinarine synergistically potentiates aminoglycoside-mediated bacterial killing. *J. Microbial. Biotechnol.* **15**, 2055–2070 (2022).

79. A. K. Cain, L. M. Nolan, G. J. Sullivan, C. B. Whitchurch, A. Filloux, J. Parkhill, Complete genome sequence of pseudomonas aeruginosa reference strain PAK. *Microbiol. Resour. Announc.* **8**, e00865-19 (2019).

80. K. Makino, K. Oshima, K. Kurokawa, K. Yokoyama, T. Uda, K. Tagomori, Y. Iijima, M. Najima, M. Nakano, A. Yamashita, Y. Kubota, S. Kimura, T. Yasunaga, T. Honda, H. Shinagawa, M. Hattori, T. Iida, Genome sequence of Vibrio parahaemolyticus: A pathogenic mechanism distinct from that of V cholerae. *Lancet* **361**, 743–749 (2003).